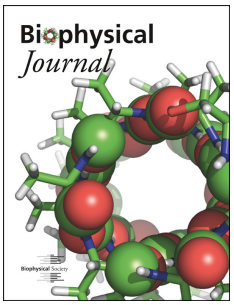


# Physical phenotype of blood cells is altered in COVID-19

Markéta Kubánková, Bettina Hohberger, Jakob Hoffmanns, Julia Fürst, Martin Herrmann, Jochen Guck, Martin Kräter

PII: S0006-3495(21)00454-9

DOI: https://doi.org/10.1016/j.bpj.2021.05.025

Reference: BPJ 11152

To appear in: *Biophysical Journal*

Received Date: 15 December 2020

Accepted Date: 27 May 2021

Please cite this article as: Kubánková M, Hohberger B, Hoffmanns J, Fürst J, Herrmann M, Guck J, Kräter M, Physical phenotype of blood cells is altered in COVID-19, *Biophysical Journal* (2021), doi: https://doi.org/10.1016/j.bpj.2021.05.025.

# Physical phenotype of blood cells is altered in COVID-19

Markéta Kubánková[1], Bettina Hohberger[2], Jakob Hoffmanns[2], Julia Fürst[3], Martin Herrmann[4,5], Jochen Guck[1,6,#], Martin Kräter[1]

[1]Max Planck Institute for the Science of Light & Max-Planck-Zentrum für Physik und Medizin, Staudtstraße 2, 91058 Erlangen, Germany
[2]Department of Ophthalmology, Friedrich-Alexander-University Erlangen-Nürnberg, Schwabachanlage 6, 91054 Erlangen, Germany
[3]Department of Internal Medicine 1, University Medical Center Erlangen, Friedrich-Alexander-University Erlangen-Nürnberg, Erlangen, Germany
[4]Department of Internal Medicine 3, University Medical Center Erlangen, Friedrich-Alexander-University Erlangen-Nürnberg, Erlangen, Germany
[5]Deutsches Zentrum Immuntherapie (DZI), Erlangen, Germany;
[6]Department of Physics, Friedrich-Alexander-University Erlangen-Nürnberg, Erlangen, Germany

# corresponding author

## Abstract

Clinical syndrome coronavirus disease 2019 (COVID-19) induced by severe acute respiratory syndrome coronavirus 2 (SARS-CoV-2) is characterized by rapid spreading and high mortality worldwide. While the pathology is not yet fully understood, hyper-inflammatory response and coagulation disorders leading to congestions of microvessels are considered to be key drivers of the still increasing death toll. Until now, physical changes of blood cells have not been considered to play a role in COVID-19 related vascular occlusion and organ damage. Here we report an evaluation of multiple physical parameters including the mechanical features of five frequent blood cell types, namely erythrocytes, lymphocytes, monocytes, neutrophils, and eosinophils. More than 4 million blood cells of 17 COVID-19 patients at different levels of severity, 24 volunteers free from infectious or inflammatory diseases, and 14 recovered COVID-19 patients were analyzed. We found significant changes in lymphocyte stiffness, monocyte size, neutrophil size and deformability, and heterogeneity of erythrocyte deformation and size. While some of these changes recovered to normal values after hospitalization, others persisted for months after hospital discharge, evidencing the long-term imprint of COVID-19 on the body.

## Significance Statement

COVID-19 can lead to the impairment of the circulatory system, including effects such as vascular occlusion and hypoxemia. The physical properties of blood cells have crucial roles for proper circulation. Quick and simple examination of these properties would accomplish an unmet clinical need for rapid diagnostics of the cell's functional status. Here we employed real-time deformability cytometry, a label free, high-throughput imaging technology to assess various physical properties of blood cells. We identified significant and persisting changes of cell size and mechanical properties in acute phase and post COVID-19. These changes might be predictive for cell functionality such as oxygen delivery. Thus, our findings have implications for COVID-19 diagnostics and treatment.

Keywords:

real-time deformability cytometry | blood cell physical phenotype | cell mechanics | cell size | immune cells | erythrocytes | coronavirus disease 2019 (COVID-19) | severe acute respiratory syndrome coronavirus 2 (SARS-CoV-2)

## Introduction

Peripheral blood is a key body fluid analyzed during the diagnostic routine, including infectious disease diagnostics. Infection by severe acute respiratory syndrome coronavirus 2 (SARS-CoV-2) may lead to the clinical syndrome coronavirus disease 2019 (COVID-19), which is accompanied by changes in numbers and phenotypes of blood cells (1). Typically, various immune cells such as T-lymphocytes, monocytes and macrophages get activated and contribute to the so-called hyper-inflammatory response (2). The uncontrolled inflammation is believed to be a major cause of disease severity and death during COVID-19 (3). Furthermore, abnormal coagulation and thrombotic events leading to vascular occlusion are described as major contributors to the high mortality (4, 5).

Apart from the biochemical state of blood cells, infectious diseases can also alter their physical properties, including morphological or mechanical features. It is long known that mechanical properties of cells can act as a disease marker, as reviewed by Di Carlo (6), and can contribute to vascular occlusion, as reviewed by Lipowsky (7). To date, a systematic evaluation of the effect of COVID-19 on the physical phenotypes of the most frequent blood cells was missing. To address this gap, we employed real-time deformability cytometry (RT-DC), a label free, high-throughput technology that allows quick image-based mechanical interrogation of cells at rates of up to 1000 cells per second (8). Previously, the technique was used to detect disease specific signatures of blood cell pathological changes in several conditions including spherocytosis, malaria, acute lymphoid leukemia, and acute myeloid leukemia (9). During viral respiratory tract infection Toepfner *et* al. reported an increase of neutrophil and monocyte size and deformability, as well as larger and more deformable lymphocytes in acute Epstein-Barr-virus infection.

Here we examine COVID-19 related changes of physical phenotype of several cell types found in peripheral blood, namely erythrocytes, lymphocytes, monocytes and neutrophils. In total, more than $4x10^6$ blood cells from 55 blood samples were analyzed, including 17 COVID-19 positive patients, 14 recovered patients, and 24 age matched volunteers showing no indication of infection or inflammatory disease. We found that COVID-19 is linked with significantly decreased lymphocyte stiffness, increased monocyte cell size, the appearance of smaller and less deformable erythrocytes, and the presence of large, deformable, activated neutrophils. Certain changes had not returned to the control group levels months after release from the hospital, bringing evidence of the long-lasting effects of COVID-19 on the circulatory system.

Our results show that real-time deformability cytometry can be used to follow the course of COVID-19 and the immune response against it. In the future, we anticipate that measurements of morphological and mechanical properties of blood cells will contribute towards improving infectious disease diagnostics.

## Materials and Methods

### Peripheral blood collection

COVID-19 patients were hospitalized with a majority at intensive care unit (ICU) of the Department of Internal Medicine 1, Friedrich-Alexander-University Erlangen-Nürnberg, Germany (FAU) showing different severity levels at the time of blood sampling. COVID-19 venous blood samples (n = 17) were taken from hospitalized patients of the Department of Internal Medicine 1, FAU, between April and May 2020. Recovered patient venous blood samples (n = 14) were taken from patients of the Department of Internal Medicine 1, FAU, and COVID-19 patients in quarantine, in recovery from COVID-19 between four and eight months after release from the hospital or quarantine (median 7.1 ± 1.1 months). All patients had positive PCR tests for COVID-19. Control venous blood samples (healthy cohort) were taken from patients of the Department of Ophthalmology, FAU (patient information can be found in Supplementary table 1). Blood was drawn using a 20-gauge multifly needle into a sodium citrate S-monovette by vacuum aspiration with the tenets of the Declaration of Helsinki. Informed written consent was obtained from all participants. All experiments were performed according to the institutional guidelines and the ethical approval of the Ethical Committee of the University Medical Center of Erlangen (permits #193_13B and #174_20B and 295_20B). After blood collection, samples were used for clinical routine diagnostics and an aliquot was taken for RT-DC analysis within the standard storing time and conditions.

### Sample preparation

Prior to measurement, 50 µl of whole blood was gently mixed with 950 µl of measurement buffer (MB) composed of 0.6% (m/v) methyl cellulose dissolved in phosphate buffered saline (PBS; Figure 1 A), adjusted to a viscosity of 60 mPa.s at 24°C using a falling ball viscometer (Haake, Thermo Scientific).

### Real-time deformability cytometry

Real-time deformability cytometry (RT-DC) measurements were performed as described previously using an AcCellerator instrument (Zellmechanik Dresden GmbH) (9). The cell suspension was loaded into a 1 ml syringe, attached to a syringe pump (neMESYS, Cetoni GmbH) and connected by PEEK-tubing (IDEX Health & Science LLC) to a microfluidic chip made of PDMS bonded on cover glass. A second syringe with sheath fluid (pure measurement buffer) was connected to the chip, which consisted of two inlets (one for the sheath fluid and one for the sample) and one outlet connected by a channel constriction of 20 × 20 µm square cross-section, where the measurement was performed. The total flow rate was 0.06 µl/s, of which the sheath flow rate was 0.045 µl/s and the sample flow rate was 0.015 µl/s. To perform a measurement, the chip was mounted on the stage of an inverted high-speed microscope equipped with a CMOS camera. Measurement temperature was 23°C. Images were acquired at a frame rate of 1600 fps. Cells were detected in a region of interest of 250 × 80 pixels and morphological and mechanical parameters were acquired in real-time (Figure 1 B).

### Data analysis

Cell images were analyzed using ShapeOut software (10) and Python 3.7 using dclab library (11). For each patient, the five studied cell populations were hand-gated in the cell brightness-area parameter plot according to the procedure described in Toepfner *et* al. (9). We applied a gate for minimum cross-sectional area (15 $\mu m^2$) and for the area ratio (1 – 1.05 for leukocytes, 1 – 1.08 for erythrocytes). The

calculation of deformation, a measure of how much the cell shape deviates from circularity, and was obtained from the image using the projected area (*A*) and cell contour length calculated from the convex hull (*l*):

$$Deformation = \frac{1 - 2\sqrt{\pi A}}{l} \quad \text{Eq. 1}$$

The calculation of the Young's modulus was done using a look-up table derived from simulations based on the finite elements method (12) and the analytical solution (13). Cell volume was computed from the event contour under the assumption of rotational symmetry with a rotational axis parallel to the flow direction. The calculation is based on a full rotation of the upper and the lower halves of the contour, which are then averaged.

Statistical analysis was done in Python 3.7 using Kruskal-Wallis *H*-test and post-hoc Dunn's test with Bonferroni correction. In graphs, *p*-values are represented by * $p < .05$, ** $p < .01$, *** $p < .001$. The effect size was estimated by the epsilon squared, $\varepsilon^2$ (14), which was calculated from the *H*-test statistic as follows (15):

$$\varepsilon_R^2 = \frac{H}{(n^2 - 1)/(n + 1)} \quad \text{Eq. 2}$$

where *H* is the Kruskal-Wallis *H*-test statistic, n is the total number of observations, and the $\varepsilon^2$ coefficient assumes the value from 0 (indicating no relationship) to 1 (perfect relationship). The effect size was interpreted according to Rea *et* Parker (16), details are found in Supplementary table 2.

For the comparison of three donors at two time points (during and post COVID-19), statistical analyses were carried out using a 1D linear mixed model that incorporates fixed effect parameters and random effects to analyze differences between cell subsets and replicate variances, respectively. *p*-values were determined by a likelihood ratio test, comparing the full model with a model lacking the fixed effect term (17), and are represented in the graphs by * $p < .05$, ** $p < .01$, *** $p < .001$.

## Data availability statement

All data acquired and used for analysis are publicly available. doi: 10.5281/zenodo.4737521

## Results

We studied the peripheral blood from 17 COVID-19 patients hospitalized at the time of sample collection (median age 68 ± 10.4 years) compared to a cohort of 24 volunteers free from infectious or inflammatory diseases (62.5 ± 13.6 years) and 14 blood donors on average 7 months after hospitalization with COVID-19 (age 58.6 ± 12.4 years, herein referred to as the 'recovered' patients). Whole blood was diluted in measurement buffer at a ratio of 1:20 and analyzed with RT-DC (Figure 1). For each patient, the five most frequent blood cell populations were manually gated according to the established analysis protocol (9): erythrocytes, lymphocytes, monocytes, neutrophils, and eosinophils.

In agreement with other studies (18, 19) we observed significant alterations of white blood cell (WBC) counts in severe COVID-19 cases, namely neutrophilia (elevated number of neutrophils) and lymphopenia (decreased number of lymphocytes), Supplementary figure 1. Here it should be noted that

reports of lymphopenia in literature are controversial, as for instance Ramonell et al. reported elevated levels of lymphocytes in COVID-19 patients (20). The median neutrophil to lymphocyte ratio (NLR) increased from 0.97 ± 0.70 to 3.62 ± 3.36, with several cases where NLR was over 8. The NLR increase calculated from RT-DC data was consistent with literature, where NLR is reported as a prognostic marker of COVID-19 mortality (21). In some patients we also observed monocytosis (22): while the proportion of monocytes to total WBC was mostly in the normal range of 2–8%, in several COVID-19 cases it reached over 10% (Supplementary figure 1). No significant changes were found in eosinophil counts. Overall these findings confirm that, purely from the images of cells obtained with RT-DC, it is possible to reproduce the results of conventional complete blood counts (9). The focus of this study, however, was the interrogation of changes of blood cell physical phenotype. The following sections describe alterations of erythrocytes and leukocytes during COVID-19. While the most striking findings are presented below, the reader will find a comprehensive overview of all the analyzed physical features for each cell type in the Supplementary information (Supplementary figure 2-6).

**COVID-19 induces the appearance of erythrocytes with distinct physical phenotype**

RT-DC analysis revealed erythrocyte anomaly in COVID-19 patients, mainly characterized by the appearance of small erythrocytes with low deformation in standardized channel flow conditions (Figure 2 A-E). The median deformation of erythrocytes exhibited a weak decrease in COVID-19 patients compared to healthy donors and recovered patients (Kruskal-Wallis $p = .22$, $\chi^2 = 3.1$, $\varepsilon^2 = 0.06$), Figure 2 F. It is noteworthy that several of the COVID-19 patients had very low median erythrocyte deformability compared to the rest of the blood donors.

Significant differences with strong effect size were observed in the standard deviations of erythrocyte deformation (Kruskal-Wallis $p < .0001$, $\chi^2 = 42.3$, $\varepsilon^2 = 0.78$), Figure 2 G. The significant broadening of the deformation distribution during COVID-19 was the result of the appearance of erythrocytes with low deformation, as shown in Figure 2 D. Such cells were rare in the healthy patient cohort.

Alongside the significant difference in standard deviation (SD) of deformation between hospitalized patients and the healthy cohort ($p < .0001$, see Supplementary table 2 for detailed results of Dunn's post-hoc tests), we also found significant differences between the recovered and hospitalized cohorts ($p = .002$) and between the recovered and healthy cohorts ($p = .03$)., Figure 2 G. Clearly, erythrocytes of the recovered patients had not fully returned to the state of the healthy cohort.

In addition to the increased SD of deformation, we also found increased SD of cell size, specifically the cross-sectional area of the image-derived cell contours and the cell volume (Supplementary figure 2). The increased standard deviations of cell size and deformation were in accordance with reported broadening of the red blood cell distribution width (RDW), a routine complete blood count component (23). Some of the cells were not only smaller than usual but also asymmetrically shaped, raising suspicion of the presence of fragmented erythrocytes. This is a valid hypothesis as schistocytes have been reported as a marker of severe COVID-19 (24).

In general, the phenotype changes observed with RT-DC may be associated with structural and functional changes. A recent study has reported that COVID-19 causes irreversible damage to the erythrocyte proteome (25). The authors found that oxidative stress connected with COVID-19 damages

essential proteins in erythrocytes, including those that influence membrane structure and the ability to transport and deliver oxygen. Since mature erythrocytes cannot synthesize new proteins to replace damaged ones and the average lifespan of erythrocytes is 120 days, the authors hypothesize that the circulation of irreversibly damaged erythrocytes with impaired function could contribute to the long-term effects of COVID-19 (25).

According to our findings, COVID-19 is connected with the appearance of less deformable erythrocytes. Cell deformability is thought to be a key factor determining splenic clearance (26) and it is likely that erythrocytes strongly deviating from normal deformability get removed by the spleen. Interestingly, we observed that erythrocyte heterogeneity in recovered patients had not fully decreased back to healthy donor levels. Thus, we hypothesize that erythrocytes with only minor deviation from normal deformability pass through the spleen unnoticed. Due do the long erythrocyte lifespan, such cells may remain in the blood circulation for months. The altered physical properties of circulating blood cells could even induce mechanical stress and impair the function of the spleen in filtering out abnormal red blood cells. These phenomena could contribute to the long-term problems experienced by many COVID-19 patients (27).

**Decreased lymphocyte stiffness in COVID-19 patients**

RT-DC analysis revealed increased deformability of peripheral blood lymphocytes during severe COVID-19 ($p$ = .013, $\chi^2$ = 8.7, with relatively strong effect size $\varepsilon^2$ = 0.16), as can be seen in Figure 3 A-E. While lymphocyte cell size did not differ among healthy donors, recovered, and hospitalized COVID-19 patients (medians 37.8 ± 1.3 μm$^2$, 38.6 ± 0.7 μm$^2$ and 39.0 ± 2 μm$^2$, respectively, Figure 3 F), lymphocyte deformation in standardized channel flow conditions was elevated during COVID-19. Compared to the healthy donor median deformation of 0.025 ± 0.006, hospitalized COVID-19 patient lymphocytes had a significantly higher median deformation 0.029 ± 0.003, $p$ = .011 (Figure 3 G). Lymphocyte deformation was 0.026 ± 0.002 for recovered patients, not significantly different from that of the control group.

The sphericity of lymphocytes under normal conditions allowed us to exploit the developed theoretical framework (13) to calculate the Young's modulus from RT-DC data. The Young's modulus, a measure of overall cell stiffness, was significantly lower in the COVID-19 cohort ($p$ = .003, $\chi^2$ = 11.7, $\varepsilon^2$ = 0.22) (Figure 3 H). While the control group median Young's modulus was 1.15 ± 0.12 kPa, it went down to 1.03 ± 0.10 kPa in hospitalized COVID-19 patients ($p$ = .003, Dunn's post-hoc test), reflecting a decrease of stiffness. The decreased Young's modulus in lymphocytes during COVID-19 was further confirmed by comparing data of three patients during and after COVID-19 (Supplementary figure 3 L). To the best of our knowledge, this study reveals the first evidence of altered mechanical properties of lymphocytes during COVID-19.

**Monocytes of COVID-19 patients exhibit a dramatic increase in cell volume**

In inflammatory disease, monocytes can contribute to the immune response either directly or via differentiation into dendritic cells or macrophages. Therefore it is not surprising that altered monocyte phenotype and function is characteristic for COVID-19 patients (1). Examination of monocytes with RT-

DC revealed a significant change in monocyte size ($p < .0001$, $\chi^2 = 30.6$, $\varepsilon^2 = 0.57$) triggered by the appearance of larger monocytes during COVID-19 (Figure 4 A-D). Monocytes of hospitalized COVID-19 patients had a median cell cross-sectional area of 70.5 ± 7.1 $\mu m^2$, significantly higher compared to recovered patients (65.0 ± 2.5 $\mu m^2$, $p < .0001$, Dunn's post-hoc test) and that of the healthy cohort, 63.8 ± 2.2 $\mu m^2$ ($p < .0001$), Figure 4 E. This represents a 9.5% increase from the median cross-sectional area of the healthy cohort. In addition, the standard deviation of cross-sectional area increased during COVID-19 ($p = .001$, $\chi^2 = 13.7$, $\varepsilon^2 = 0.25$) due to the appearance of large monocytes (Figure 4 F).

The differences in cell volume were also pronounced ($p < .0001$, $\chi^2 = 27.7$, $\varepsilon^2 = 0.51$) with a 16.7% increase of median cell volume during COVID-19. The median volume of COVID-19 patient monocytes was 353.7 ± 55.8 $\mu m^3$ compared to 303.2 ± 12.0 $\mu m^3$ for the healthy cohort and 304.9 ± 19.4 $\mu m^3$ for recovered patients (Figure 4 G). Assuming spherical shape, this would correspond to monocyte diameters of 8.8 µm for COVID-19 patients and 8.3 µm for healthy donors. Again, the standard deviation of cell volume was significantly higher for COVID-19 patients ($p < .0001$, $\chi^2 = 18.5$, $\varepsilon^2 = 0.34$), as shown in Figure 4 H. The observed size changes could be due to the appearance of a subpopulation of large, possibly highly phagocytic monocytes (28). Morphological anomaly of COVID-19 patient monocytes has been observed by Zhang *et* al. (29). In their study, monocyte size was assessed indirectly using flow cytometry forward scatter (FSC). Unlike RT-DC, FSC measurement does not quantify absolute size changes (30). Still, the authors were able to observe a relative change of monocyte size and reported an increase in COVID-19 compared to healthy individuals, in line with our observation. In their study, the FSC-high population was more pronounced in patients requiring hospitalization and ICU admission.

No significant differences in deformation or Young's modulus were found among the three studied groups (Supplementary figure 4), proving that the stiffness of monocytes remained unchanged during COVID-19.

**Altered physical phenotype signals neutrophil activation in COVID-19**

Finally, RT-DC analysis provided evidence of significant changes with strong effect sizes in neutrophil cross-sectional area ($p < .0001$, $\chi^2 = 23.0$, $\varepsilon^2 = 0.43$), volume ($p < .0001$, $\chi^2 = 23.5$, $\varepsilon^2 = 0.44$) and deformation ($p = .0013$, $\chi^2 = 13.3$, $\varepsilon^2 = 0.25$), Figure 5. During COVID-19, neutrophils were on average larger (68.7 ± 3.5 $\mu m^2$ vs. healthy donors 63.5 ± 2.2 $\mu m^2$, $p < .0001$), had higher volume (327.5 ± 27.2 $\mu m^3$ vs. healthy donors 292.0 ± 12.9 $\mu m^3$, $p < .0001$) and were more deformed under the standard capillary flow conditions in RT-DC (0.059 ± 0.009 vs. healthy donors 0.051 ± 0.004, $p = 0.002$), Figure 5 F-H. The standard deviations of neutrophil cross-sectional area, volume and deformation were also significantly higher in the COVID-19 patients compared to healthy individuals (Supplementary figure 5), reflecting higher heterogeneity in the population of neutrophils.

We hypothesize that the described changes of physical properties observed with RT-DC are linked to an activated state of neutrophils. The joint increase of size and deformation of stimulated neutrophils *in vitro* and *in vivo* has been documented by RT-DC analysis previously (9, 31). Change in these parameters could serve as a proxy readout for neutrophil activation. The underlying mechanism is still unclear, although it has been reported that the volume of activated neutrophils increases through connected Na+/H+ antiport activity (32). Our observations can also reflect the fact that in severe COVID-19,

strongly activated neutrophils may adopt a so-called low-density phenotype which is prone to neutrophil extracellular trap (NET) formation (33). The lower density of this population of neutrophils could be logically linked with the elevated size and deformability observed with RT-DC. The process was reported as a source of vascular occlusion, possibly leading to vascular damage and organ dysfunction in COVID-19 (33).

The median Young's modulus calculated from RT-DC data exhibited a weak decrease during COVID-19 (Figure 5 I), revealing that neutrophils were generally less stiff in COVID-19 patients. These changes of Young's modulus were further confirmed by comparing data of three patients during and after COVID-19 (Figure 5 J), demonstrating a clear decrease of neutrophil stiffness during COVID-19.

Interestingly, in recovered patients, neutrophil parameters (cross-sectional cell area 66.2 ± 2.5 $\mu m^2$, volume 308.9 ± 15.3 $\mu m^3$, deformation 0.055 ± 0.005) had not returned to the values of the healthy cohort (Figure 5 F-H). Carissimo *et* al. found that the neutrophil counts per defined volume of blood in recovered patients did not fully return to values of healthy individuals (34). Together with our findings, this suggests that COVID-19 infection leaves a lasting influence on the immune system.

In addition to neutrophils, we also examined a different group of granulocytes, eosinophils. Eosinophils are known to react to certain viral infections of the respiratory system *in vitro* and *in vivo*, including respiratory syncytial virus and influenza (35, 36). However, eosinophils did not show any changes of their physical phenotype during infection or in recovered state (Supplementary figure 6).

The above findings were reported as the medians and standard deviations of three mostly independent cohorts of blood donors. For three of the patients we performed RT-DC measurements both during COVID-19 and after recovery, and could therefore directly examine the progression of blood cell parameters in a single individual. The comparison of various blood cell features of these three donors at the two studied time points can be found in Supplementary figures 2-6. The trends confirm what we describe in the text above: severe COVID-19 is linked with the presence of erythrocytes with distinct phenotype and lower deformation, larger monocytes, softer lymphocytes and larger, more deformed neutrophils.

## Discussion

In our study, the physical parameters of blood cells including mechanical properties act as sensitive reporters of pathophysiological changes in COVID-19 patients compared to age-matched controls. The concept that cell morphology and mechanics are inherent markers of cell function has long been established (37, 38). Using RT-DC, we were able to monitor the physical properties of cells from whole blood without the need for tedious preparation or enrichment. In COVID-19 patients we found alterations of erythrocytes and leukocyte subsets with the potential to be exploited as diagnostic markers. This paves the way for high-speed, label-free and cost-effective disease detection. We note that the relatively low number of COVID samples included in our study and the huge space of possible cellular responses to viral infection makes it a necessity to acquire many more RT-DC datasets to ensure the specificity of an observed pattern for a particular disease. In the context of limited existing RT-DC data on viral infections, the blood cell response to COVID-19 was unique. In a previous study, neutrophils derived from patients with viral respiratory tract (RTI) and Epstein-Barr-virus (EBV) infection exhibited similar changes in cell size and deformation as what we observed for COVID-19 (9). In RTI and EBV, monocytes were larger and significantly more deformable than the controls, while in COVID-19

monocyte deformation did not change. Lymphocytes showed distinct responses to the three viral infections: in COVID-19 they were more deformable, in RTI showed no changes, and in EBV the lymphocytes were bigger and more deformable compared to controls (9). In the future, RT-DC could be of high significance for the fast identification of a specific infection of viral or other origin. This would be an advantage in times when molecular diagnostic tests such as qPCR become inaccessible, such as during critical phases of a pandemic.

A key finding of our study was that the erythrocytes of COVID-19 patients were significantly more heterogeneous in size and deformation under constant shear stress, compared to healthy controls. In a recent report, Thomas et al. identified structural protein damage and membrane lipid remodeling in erythrocytes as potential causes of impaired oxygen delivery during COVID-19 (25). These changes could be linked with the altered physical properties of the cells, as the composition and properties of plasma membranes interplay with the cytoskeleton to regulate physical properties of cells such as shape (39). The physical properties of erythrocytes are crucial for microcirculatory flow (40, 41) and as such, these changes could impair circulation and promote hypoxemia. The effect could persist in COVID-19 patients long after the infection is not active anymore; we found that in recovered patients phenotype alterations were not as prominent, but still present. A different explanation for the persistence of less deformable erythrocytes in recovered patients could be that the cells already had a different physical phenotype before clinical onset. Altered mechanical properties of cells due to factors such as age could increase susceptibility to SARS-CoV-2 infection, as suggested by Uhler and Shivashankar (42).

While erythrocytes are present in high quantities (three orders of magnitude more frequent than leukocytes), also the numbers and physical features of leukocytes are crucial for proper blood flow (43). RT-DC provides direct access to relative leukocyte counts, their size and mechanical properties. In accordance with other studies (19, 44) we found neutrophilia and lymphopenia as well as increased neutrophil to lymphocyte ratio in COVID-19 patients. Importantly, we report on changes of size and mechanical properties of leukocyte subsets in COVID-19 samples. These changes might be key to understanding vessel occlusion and pulmonary embolism, as the interrogation of cell morphology and mechanics in former studies established the importance of these factors for cell circulation under physical (45), pathological (46, 47), and artificial (48) conditions.

We hypothesize that the observed changes could arise due to cytoskeletal alterations of immune cells. Mechanical properties of cells can be directly related to the cytoskeleton (37, 38, 49, 50), an important supportive structure which also determines cellular function (51–54). Previously, RT-DC allowed us to detect actin cytoskeletal rearrangements during rubella virus infection, which correlated with an altered cell shape and reduced migratory potential (55). Although it is known that viruses can use immune cells as vehicles to travel the body (56) and hijack the actin cytoskeleton (57), viral traces were absent in the blood of COVID-19 patients (58). However, the cytoskeleton may be affected by the infection indirectly *e.g.* through the involvement of cytoskeleton-dependent signaling (59). Hyperinflammation and cytokine storm syndrome are reported in COVID-19 cases with high levels of macrophage inflammatory protein 1-α, granulocyte-colony stimulating factor (G-CSF), interleukins IL-2 and IL-7, interferon-γ inducible protein 10, monocyte chemoattractant protein 1, and tumour necrosis factor-α (TNF) (60). Such cytokines were reported to induce cytoskeletal changes in myeloid cells and to interfere with their physical phenotypes during immune function (61–63). For example, Kutsuna et al. found actin depolymerization and changes of cell morphology upon treating neutrophils with TNF, G-CSF and GM-CSF (61), suggesting cell softening. In an RT-DC study, GM-CSF was found to activate neutrophils and induce similar size and

deformation changes to what we have seen for neutrophils from COVID-19 patients (31). This leads us to speculate on the possible role of cytokines in triggering cytoskeletal reorganization and physical changes of immune cells during COVID-19.

We are aware of certain limitations of our study, *e.g.* that it falls short of representative patient cohorts to compare mild with critical symptoms. Still, we were able to identify changes of blood cell physical phenotypes that did not return to the baseline healthy donor levels several months after SARS-CoV-2 infection, namely in erythrocytes and neutrophils. It is important to mention that neutrophils are short lived cells with an average lifespan of less than one day. Thus, neutrophil alterations observed in our recovered cohort were induced after the *after* the successful displacement of the virus by the immune system. This might be indicative for SARS-CoV-2 causing long-term immunological signals or even targeting bone marrow stem cells, as viral RNA was found *post-mortem* in patient bone marrow (64).

The persistent alterations of erythrocytes and neutrophils could be connected with long term symptoms of the recovered patients, of which 70% described chronic headache or neurological symptoms, 54% had concentration disorders and 62% circulatory problems like cold sweat and tachycardia. We hypothesize that the persisting changes of blood cell physical phenotypes could contribute to the long-term impairment of circulation and oxygen delivery linked with COVID-19 (17).

Lastly, we would like to add a speculative thought on cell physical changes as a tightly regulated mechanism by which the body controls the circulation or extravasation of immune cells. Fay et al. reported in 2016 that cellular softening mediates leukocyte demargination and trafficking, thereby increasing clinical blood counts (45). It is possible that in similar manner, cell size contributes to the effective cell circulation. If a cell is smaller or more deformable, it could circulate better through narrow capillaries compared to a bigger or stiffer one. Thus, precise cell size or mechanics adaptations could control the retention of leukocytes in tissue capillaries and subsequently lead to extravasation.

Taken together, label-free physical phenotyping of blood cells with real-time deformability cytometry provides a fast, sensitive and unbiased way to feel for functional changes in cells. As such, deformability cytometry data has the potential to be used as a biomarker of COVID-19 and potentially other infectious diseases. In the future, RT-DC could be part of the first line of defense against an unknown virus during a pandemic.

## Acknowledgements

The authors would like to thank Leonie Staats and Aylin Lindemann for technical assistance and Despina Soteriou, Michael Moritz, Charlotte Szewczykowski, and Folkert Horn for study support.

## Author contributions

M.K., J.G., and M.K. designed the project outline and carried out experiments, interpreted results, and wrote the initial manuscript. B.H., M.H. provided samples and patient information, interpreted and discussed results, and co-wrote the manuscript. J.H. and J.F. provided samples and patient information and co-wrote the manuscript.

## Conflict of interest

The authors declare no conflict of interest.

## References

1. Mann, E.R., M. Menon, S.B. Knight, J.E. Konkel, C. Jagger, T.N. Shaw, S. Krishnan, M. Rattray, A. Ustianowski, N. Diar Bakerly, P. Dark, G.M. Lord, A. Simpson, T. Felton, L.-P. Ho, NIHR Respiratory TRC, M. Feldmann, CIRCO, J.R. Grainger, and T. Hussell. 2020. Longitudinal immune profiling reveals key myeloid signatures associated with COVID-19. *Sci. Immunol*. 5.

2. Tay, M.Z., C.M. Poh, L. Rénia, P.A. MacAry, and L.F.P. Ng. 2020. The trinity of COVID-19: immunity, inflammation and intervention. *Nat. Rev. Immunol.* 20:363–374.

3. Mehta, P., D.F. McAuley, M. Brown, E. Sanchez, R.S. Tattersall, and J.J. Manson. 2020. COVID-19: consider cytokine storm syndromes and immunosuppression. *Lancet*. 395:1033–1034.

4. Tang, N., D. Li, X. Wang, and Z. Sun. 2020. Abnormal coagulation parameters are associated with poor prognosis in patients with novel coronavirus pneumonia. *J. Thromb. Haemost.* 18:844–847.

5. Chen, N., M. Zhou, X. Dong, J. Qu, F. Gong, Y. Han, Y. Qiu, J. Wang, Y. Liu, Y. Wei, J. Xia, T. Yu, X. Zhang, and L. Zhang. 2020. Epidemiological and clinical characteristics of 99 cases of 2019 novel coronavirus pneumonia in Wuhan, China: a descriptive study. *Lancet*. 395:507–513.

6. Di Carlo, D. 2012. A mechanical biomarker of cell state in medicine. *J. Lab. Autom.* 17:32–42.

7. Lipowsky, H.H. 2005. Microvascular rheology and hemodynamics. *Microcirculation*. 12:5–15.

8. Otto, O., P. Rosendahl, A. Mietke, S. Golfier, C. Herold, D. Klaue, S. Girardo, S. Pagliara, A. Ekpenyong, A. Jacobi, M. Wobus, N. Töpfner, U.F. Keyser, J. Mansfeld, E. Fischer-Friedrich, and J. Guck. 2015. Real-time deformability cytometry: On-the-fly cell mechanical phenotyping. *Nat. Methods*. 12:199–202.

9. Toepfner, N., C. Herold, O. Otto, P. Rosendahl, A. Jacobi, M. Kräter, J. Stächele, L. Menschner, M. Herbig, L. Ciuffreda, L. Ranford-Cartwright, M. Grzybek, Ü. Coskun, E. Reithuber, G. Garriss, P. Mellroth, B. Henriques-Normark, N. Tregay, M. Suttorp, M. Bornhäuser, E.R. Chilvers, R. Berner, and J. Guck. 2018. Detection of human disease conditions by single-cell morpho-rheological phenotyping of blood. *Elife*. 7.

10. Paul Müller and others. 2019. Shape-Out version 2.3.0: Analysis software for real-time deformability cytometry [Software]. Available at https://github.com/ZELLMECHANIK-DRESDEN/ShapeOut2. .

11. Paul Müller and others. 2015. dclab version 0.31.2: Python library for the post-measurement analysis of real-time deformability cytometry data sets [Software]. Available at https://github.com/ZELLMECHANIK-DRESDEN/dclab. .

12. Mokbel, M., D. Mokbel, A. Mietke, N. Träber, S. Girardo, O. Otto, J. Guck, and S. Aland. 2017. Numerical Simulation of Real-Time Deformability Cytometry to Extract Cell Mechanical

Properties. *ACS Biomater. Sci. Eng.* 3:2962–2973.

13. Mietke, A., O. Otto, S. Girardo, P. Rosendahl, A. Taubenberger, S. Golfier, E. Ulbricht, S. Aland, J. Guck, and E. Fischer-Friedrich. 2015. Extracting Cell Stiffness from Real-Time Deformability Cytometry: Theory and Experiment. *Biophys. J.* 109:2023–2036.

14. Kelley, T.L. 1935. An Unbiased Correlation Ratio Measure. *Proc. Natl. Acad. Sci.* 21:554–559.

15. Tomczak, M., and E. Tomczak. 2014. The need to report effect size estimates revisited. An overview of some recommended measures of effect size. *Trends Sport Sci.* 1:19–25.

16. Rea, L.M., and R.A. Parker. 2014. Designing and conducting survey research A Comprehensive Guide. Wiley.

17. Herbig, M., A. Mietke, P. Müller, and O. Otto. 2018. Statistics for real-time deformability cytometry: Clustering, dimensionality reduction, and significance testing. *Biomicrofluidics*. 12.

18. Wang, D., B. Hu, C. Hu, F. Zhu, X. Liu, J. Zhang, B. Wang, H. Xiang, Z. Cheng, Y. Xiong, Y. Zhao, Y. Li, X. Wang, and Z. Peng. 2020. Clinical Characteristics of 138 Hospitalized Patients with 2019 Novel Coronavirus-Infected Pneumonia in Wuhan, China. *JAMA - J. Am. Med. Assoc.* 323:1061–1069.

19. Tan, L., Q. Wang, D. Zhang, J. Ding, Q. Huang, Y.Q. Tang, Q. Wang, and H. Miao. 2020. Lymphopenia predicts disease severity of COVID-19: a descriptive and predictive study. *Signal Transduct. Target. Ther.* 5.

20. Woodruff, M.C., R.P. Ramonell, D.C. Nguyen, K.S. Cashman, A.S. Saini, N.S. Haddad, A.M. Ley, S. Kyu, J.C. Howell, T. Ozturk, S. Lee, N. Suryadevara, J.B. Case, R. Bugrovsky, W. Chen, J. Estrada, A. Morrison-Porter, A. Derrico, F.A. Anam, M. Sharma, H.M. Wu, S.N. Le, S.A. Jenks, C.M. Tipton, B. Staitieh, J.L. Daiss, E. Ghosn, M.S. Diamond, R.H. Carnahan, J.E. Crowe, W.T. Hu, F.E.H. Lee, and I. Sanz. 2020. Extrafollicular B cell responses correlate with neutralizing antibodies and morbidity in COVID-19. *Nat. Immunol.* 21:1506–1516.

21. Liu, Y., X. Du, J. Chen, Y. Jin, L. Peng, H.H.X. Wang, M. Luo, L. Chen, and Y. Zhao. 2020. Neutrophil-to-lymphocyte ratio as an independent risk factor for mortality in hospitalized patients with COVID-19. *J. Infect.* 81:e6–e12.

22. Mei, Y., S.E. Weinberg, L. Zhao, A. Frink, C. Qi, A. Behdad, and P. Ji. 2020. Risk stratification of hospitalized COVID-19 patients through comparative studies of laboratory results with influenza. *EClinicalMedicine*. 26:100475.

23. Foy, B.H., J.C.T. Carlson, E. Reinertsen, R. Padros I Valls, R. Pallares Lopez, E. Palanques-Tost, C. Mow, M.B. Westover, A.D. Aguirre, and J.M. Higgins. 2020. Association of Red Blood Cell Distribution Width With Mortality Risk in Hospitalized Adults With SARS-CoV-2 Infection. *JAMA Netw. open*. 3:e2022058.

24. Della Rocca, D.G., M. Magnocavallo, C. Lavalle, J. Romero, G.B. Forleo, N. Tarantino, C. Chimenti, I. Alviz, M.T. Gamero, M.J. Garcia, L. Di Biase, and A. Natale. 2020. Evidence of systemic endothelial injury and microthrombosis in hospitalized COVID-19 patients at different stages of the disease. *J. Thromb. Thrombolysis*. 51:571–576.

25. Thomas, T., D. Stefanoni, M. Dzieciatkowska, A. Issaian, T. Nemkov, R.C. Hill, R.O. Francis, K.E. Hudson, P.W. Buehler, J.C. Zimring, E.A. Hod, K.C. Hansen, S.L. Spitalnik, and A. D'alessandro. 2020. Evidence of Structural Protein Damage and Membrane Lipid Remodeling in Red Blood Cells

from COVID-19 Patients. *J. Proteome Res.*

26. Huisjes, R., A. Bogdanova, W.W. van Solinge, R.M. Schiffelers, L. Kaestner, and R. van Wijk. 2018. Squeezing for life - Properties of red blood cell deformability. *Front. Physiol.* 9:656.

27. Weerahandi, H., K.A. Hochman, E. Simon, C. Blaum, J. Chodosh, E. Duan, K. Garry, T. Kahan, S. Karmen-Tuohy, H. Karpel, F. Mendoza, A.M. Prete, L. Quintana, J. Rutishauser, L. Santos Martinez, K. Shah, S. Sharma, E. Simon, A. Stirniman, and L. Horwitz. 2020. Post-discharge health status and symptoms in patients with severe COVID-19. *medRxiv Prepr. Serv. Heal. Sci.* 646–501.

28. Wang, S.Y., K.L. Mak, L.Y. Chen, M.P. Chou, and C.K. Ho. 1992. Heterogeneity of human blood monocyte: two subpopulations with different sizes, phenotypes and functions. *Immunology*. 77:298–303.

29. Zhang, D., R. Guo, L. Lei, H. Liu, Y. Wang, Y. Wang, H. Qian, T. Dai, T. Zhang, Y. Lai, J. Wang, Z. Liu, T. Chen, A. He, M. O'Dwyer, and J. Hu. 2020. COVID-19 infection induces readily detectable morphologic and inflammation-related phenotypic changes in peripheral blood monocytes. *J. Leukoc. Biol.* JLB.4HI0720-470R.

30. Nawaz, A.A., M. Urbanska, M. Herbig, M. Nötzel, M. Kräter, P. Rosendahl, C. Herold, N. Toepfner, M. Kubánková, R. Goswami, S. Abuhattum, F. Reichel, P. Müller, A. Taubenberger, S. Girardo, A. Jacobi, and J. Guck. 2020. Intelligent image-based deformation-assisted cell sorting with molecular specificity. *Nat. Methods*. 17:595–599.

31. Bashant, K.R., A. Vassallo, C. Herold, R. Berner, L. Menschner, J. Subburayalu, M.J. Kaplan, C. Summers, J. Guck, E.R. Chilvers, and N. Toepfner. 2019. Real-time deformability cytometry reveals sequential contraction and expansion during neutrophil priming. *J. Leukoc. Biol.* 105:1143–1153.

32. Hayashi, H., O. Aharonovitz, R.T. Alexander, N. Touret, W. Furuya, J. Orlowski, and S. Grinstein. 2008. $Na^+/H^+$ exchange and pH regulation in the control of neutrophil chemokinesis and chemotaxis. *Am. J. Physiol. Physiol.* 294:C526–C534.

33. Leppkes, M., J. Knopf, E. Naschberger, A. Lindemann, J. Singh, I. Herrmann, M. Stürzl, L. Staats, A. Mahajan, C. Schauer, A.N. Kremer, S. Völkl, K. Amann, K. Evert, C. Falkeis, A. Wehrfritz, R.J. Rieker, A. Hartmann, A.E. Kremer, M.F. Neurath, L.E. Muñoz, G. Schett, and M. Herrmann. 2020. Vascular occlusion by neutrophil extracellular traps in COVID-19. *EBioMedicine*. 58.

34. Carissimo, G., W. Xu, I. Kwok, M.Y. Abdad, Y.H. Chan, S.W. Fong, K.J. Puan, C.Y.P. Lee, N.K.W. Yeo, S.N. Amrun, R.S.L. Chee, W. How, S. Chan, B.E. Fan, A.K. Andiappan, B. Lee, O. Rötzschke, B.E. Young, Y.S. Leo, D.C. Lye, L. Renia, L.G. Ng, A. Larbi, and L.F. Ng. 2020. Whole blood immunophenotyping uncovers immature neutrophil-to-VD2 T-cell ratio as an early marker for severe COVID-19. *Nat. Commun.* 11.

35. Phipps, S., C. En Lam, S. Mahalingam, M. Newhouse, R. Ramirez, H.F. Rosenberg, P.S. Foster, and K.I. Matthaei. 2007. Eosinophils contribute to innate antiviral immunity and promote clearance of respiratory syncytial virus. *Blood*. 110:1578–1586.

36. Flores-Torres, A.S., M.C. Salinas-Carmona, E. Salinas, and A.G. Rosas-Taraco. 2019. Eosinophils - Respiratory Viruses. *Viral Immunol.* 32:198–207.

37. Fletcher, D.A., and R.D. Mullins. 2010. Cell mechanics and the cytoskeleton. *Nature*. 463:485–492.

483 38. Kasza, K.E., A.C. Rowat, J. Liu, T.E. Angelini, C.P. Brangwynne, G.H. Koenderink, and D.A. Weitz.
484 2007. The cell as a material. *Curr. Opin. Cell Biol.* 19:101–107.

485 39. Diz-Muñoz, A., D.A. Fletcher, and O.D. Weiner. 2013. Use the force: Membrane tension as an
486 organizer of cell shape and motility. *Trends Cell Biol.* 23:47–53.

487 40. Lanotte, L., J. Mauer, S. Mendez, D.A. Fedosov, J.-M. Fromental, V. Claveria, F. Nicoud, G.
488 Gompper, and M. Abkarian. 2016. Red cells' dynamic morphologies govern blood shear thinning
489 under microcirculatory flow conditions. *Proc. Natl. Acad. Sci.* 201608074.

490 41. Reichel, F., J. Mauer, A.A. Nawaz, G. Gompper, J. Guck, and D.A. Fedosov. 2019. High-Throughput
491 Microfluidic Characterization of Erythrocyte Shapes and Mechanical Variability. *Biophys. J.*
492 117:14–24.

493 42. Uhler, C., and G. V. Shivashankar. 2020. Mechano-genomic regulation of coronaviruses and its
494 interplay with ageing. *Nat. Rev. Mol. Cell Biol.* 21:247–248.

495 43. Qiu, Y., D.R. Myers, and W.A. Lam. 2019. The biophysics and mechanics of blood from a materials
496 perspective. *Nat. Rev. Mater.* 1.

497 44. Wang, D., B. Hu, C. Hu, F. Zhu, X. Liu, J. Zhang, B. Wang, H. Xiang, Z. Cheng, Y. Xiong, Y. Zhao, Y. Li,
498 X. Wang, and Z. Peng. 2020. Clinical Characteristics of 138 Hospitalized Patients with 2019 Novel
499 Coronavirus-Infected Pneumonia in Wuhan, China. *JAMA - J. Am. Med. Assoc.* 323:1061–1069.

500 45. Fay, M.E., D.R. Myers, A. Kumar, C.T. Turbyfield, R. Byler, K. Crawford, R.G. Mannino, A.
501 Laohapant, E.A. Tyburski, Y. Sakurai, M.J. Rosenbluth, N.A. Switz, T.A. Sulchek, M.D. Graham, and
502 W.A. Lam. 2016. Cellular softening mediates leukocyte demargination and trafficking, thereby
503 increasing clinical blood counts. *Proc. Natl. Acad. Sci. U. S. A.* 113:1987–1992.

504 46. Rosenbluth, M.J., W. a Lam, and D. a Fletcher. 2008. Analyzing cell mechanics in hematologic
505 diseases with microfluidic biophysical flow cytometry. *Lab Chip*. 8:1062–1070.

506 47. Lam, W.A., M.J. Rosenbluth, and D.A. Fletcher. 2008. Increased leukaemia cell stiffness is
507 associated with symptoms of leucostasis in paediatric acute lymphoblastic leukaemia. *Br. J.*
508 *Haematol.* 142:497–501.

509 48. Tietze, S., M. Kräter, A. Jacobi, A. Taubenberger, M. Herbig, R. Wehner, M. Schmitz, O. Otto, C.
510 List, B. Kaya, M. Wobus, M. Bornhäuser, and J. Guck. 2019. Spheroid Culture of Mesenchymal
511 Stromal Cells Results in Morphorheological Properties Appropriate for Improved
512 Microcirculation. *Adv. Sci.* 1802104.

513 49. Bausch, A.R., and K. Kroy. 2006. A bottom-up approach to cell mechanics. *Nat. Phys.* 2:231–238.

514 50. Pegoraro, A.F., P. Janmey, and D.A. Weitz. 2017. Mechanical Properties of the Cytoskeleton and
515 Cells. *Cold Spring Harb. Perspect. Biol.* 9.

516 51. Szymanski, D., and C.J. Staiger. 2020. The Actin Cytoskeleton : Functional Arrays for Cytoplasmic
517 Organization and Cell Shape Control 1. *Plant Physiol.* 176:106–118.

518 52. Fais, S., F. Luciani, M. Logoui, S. Parlatol, and F. Lozupone. 2000. Linkage between cell membrane
519 proteins and actin-based cytoskeleton : the cytoskeletal-driven cellular functions. *Histol.*
520 *Histopathol.* 539–549.

521 53. Etienne-Manneville, S. 2004. Actin and Microtubules in Cell Motility : Which One is in Control ?

*Traffic*. 5:470–477.

54. Pollard, T.D., G.G. Borisy, and N. Haven. 2003. Cellular Motility Driven by Assembly and Disassembly of Actin Filaments. *Cell*. 112:453–465.

55. Kräter, M., J. Sapudom, N. Bilz, T. Pompe, J. Guck, and C. Claus. 2018. Alterations in Cell Mechanics by Actin Cytoskeletal Changes Correlate with Strain-Specific Rubella Virus Phenotypes for Cell Migration and Induction of Apoptosis. *Cells*. 7:136.

56. Fackler, O.T., T.T. Murooka, A. Imle, and T.R. Mempel. 2014. Adding new dimensions: Towards an integrative understanding of HIV-1 spread. *Nat. Rev. Microbiol.* 12:563–571.

57. Döhner, K., and B. Sodeik. 2004. The role of the cytoskeleton during viral infection. *Curr. Top. Microbiol. Immunol.* 285:67–108.

58. Wölfel, R., V.M. Corman, W. Guggemos, M. Seilmaier, S. Zange, M.A. Müller, D. Niemeyer, T.C. Jones, P. Vollmar, C. Rothe, M. Hoelscher, T. Bleicker, S. Brünink, J. Schneider, R. Ehmann, K. Zwirglmaier, C. Drosten, and C. Wendtner. 2020. Virological assessment of hospitalized patients with COVID-2019. *Nature*. 581:465–469.

59. Janmey, P.A. 1998. The cytoskeleton and cell signaling: Component localization and mechanical coupling. *Physiol. Rev.* 78:763–781.

60. Huang, C., Y. Wang, X. Li, L. Ren, J. Zhao, Y. Hu, L. Zhang, G. Fan, J. Xu, X. Gu, Z. Cheng, T. Yu, J. Xia, Y. Wei, W. Wu, X. Xie, W. Yin, H. Li, M. Liu, Y. Xiao, H. Gao, L. Guo, J. Xie, G. Wang, R. Jiang, Z. Gao, Q. Jin, J. Wang, and B. Cao. 2020. Clinical features of patients infected with 2019 novel coronavirus in Wuhan, China. *Lancet*. 395:497–506.

61. Kutsuna, H., K. Suzuki, N. Kamata, T. Kato, F. Hato, K. Mizuno, H. Kobayashi, M. Ishii, and S. Kitagawa. 2004. Actin reorganization and morphological changes in human neutrophils stimulated by TNF, GM-CSF, and G-CSF: the role of MAP kinases. *Am. J. Physiol. Physiol.* 286:C55–C64.

62. Girard, D., M.E. Paquet, R. Paquin, and A.D. Beaulieu. 1996. Differential effects of interleukin-15 (IL-15) and IL-2 on human neutrophils: Modulation of phagocytosis, cytoskeleton rearrangement, gene expression, and apoptosis by IL-15. *Blood*. 88:3176–3184.

63. Bashant, K.R., N. Toepfner, C.J. Day, N.N. Mehta, M.J. Kaplan, C. Summers, J. Guck, and E.R. Chilvers. 2020. The mechanics of myeloid cells. *Biol. Cell*. 1–10.

64. Stefanie Deinhardt-Emmer, D. Wittschieber, J. Sanft, S. Kleemann, S. Elschner, K.F. Haupt, V. Vau, C. Häring, J. Rödel, A. Henke, C. Ehrhardt, M. Bauer, M. Philipp, N. Gaßler, S. Nietzsche, B. Löffler, and G. Mall. 2020. Early postmortem mapping of SARS-CoV-2 RNA in patients with COVID-19 and correlation to tissue damage. *bioRxiv*.

## Figure captions

**Figure 1. Scheme of an RT-DC measurement of a peripheral blood sample.** 50 µl of venous citrate-anticoagulated blood is diluted and mixed gently in 950 µl of measurement buffer consisting of PBS and

methyl cellulose. The blood cell suspension is pumped through a microfluidic chip mounted on an inverted microscope and single cell images are processed in real-time to obtain the physical parameters of each cell. During post-processing, cell populations of interest are manually gated according to brightness and the physical properties of each population are analyzed.

**Figure 2. Decreased size and deformability of erythrocytes of hospitalized COVID-19 patients.** Typical scatter plot of erythrocyte deformation vs. cell size (cross-sectional area) of a healthy blood donor with no known viral infection (A) compared to a patient four months after undergoing COVID-19 (B) and a patient with COVID-19 in an intensive care unit (C). The erythrocytes shown in (D) are representative images of cells in the clusters marked by corresponding numbers in the scatter plot. (E) Kernel density estimate plots demonstrating the differences in cell size and deformability between the three donors (A-C). The comparison of median values of deformation (F) and standard deviation of deformation (G) between the control group of blood donors (n = 24), recovered patients (n = 14), and patients hospitalized with COVID-19 (n = 17). Statistical comparisons were done using Kruskal-Wallis test with Dunn's posthoc test, * $p < .05$, ** $p < .01$, *** $p < .001$.

**Figure 3. Lymphocytes are less stiff in peripheral blood of hospitalized COVID-19 patients.** Typical scatter plot of lymphocyte deformation vs. cell size (cross-sectional area) of a healthy blood donor with no known viral infection (A) compared to a patient four months after undergoing COVID-19 (B) and a patient with COVID-19 in an intensive care unit (C). (D) Kernel density estimate plots demonstrating the differences in cell size and deformation among the three donors (A-C). (E) Representative images of cells in the clusters marked by corresponding numbers in the scatter plots. (F) No significant differences in lymphocyte cell size were found between healthy blood donors (grey, n = 24), recovered patients approximately five months after undergoing COVID-19 (green, n = 14), and patients hospitalized with COVID-19 (yellow, n = 17). (G) Lymphocytes exhibit significantly increased deformation in hospitalized COVID-19 patients. (H) Young's modulus of lymphocytes is significantly higher in COVID-19 patients compared to the healthy or recovered donors. Statistical comparisons were done using Kruskal-Wallis test with Dunn's posthoc test, * $p < .05$, ** $p < .01$, *** $p < .001$.

**Figure 4. The appearance of large monocytes in COVID-19 patients.** Typical scatter plot of monocyte deformation vs. cell size (cross-sectional area) of a healthy blood donor with no known viral infection (A) compared to a patient four months after undergoing COVID-19 (B) and a patient with COVID-19 in an intensive care unit (C). (D) The images of cells marked by corresponding numbers in the scatter plots. (E) Kernel density estimate plots demonstrating the differences in cell size and deformation among the three donors (A-C). (F) The median monocyte cell volume is significantly elevated in hospitalized COVID-19 patients (yellow, n = 17) compared to healthy blood donors (grey, n = 24) and recovered patients (green, n = 14). (G) A significant increase is also observed in the standard deviation of cell volume. Statistical comparisons were done using Kruskal-Wallis test with Dunn's posthoc test, * $p < .05$, ** $p < .01$, *** $p < .001$.

595 **Figure 5. Altered physical phenotype of neutrophils in the peripheral blood of COVID-19 patients.**
596 Typical scatter plot of neutrophil deformation vs. cell size (cross-sectional area) of a healthy blood donor
597 with no known viral infection (A) compared to a patient four months after undergoing COVID-19 (B) and
598 a patient with COVID-19 in an intensive care unit (C). (D) Images of neutrophils marked by corresponding
599 numbers in the scatter plots. (E) Kernel density estimate plots demonstrating the differences in cell size
600 and deformation among the three donors (A-C). (F) The median cross-sectional area and (G) median cell
601 volume of neutrophils of patients hospitalized with COVID-19 (yellow, n = 17) are significantly higher
602 than that of the healthy blood donors (grey, n = 24) and of recovered patients approximately five
603 months after undergoing COVID-19 (green, n = 14). (H) Neutrophils exhibit increased deformability in
604 hospitalized COVID-19 patients compared to the healthy cohort (I) Young's modulus of neutrophils of
605 the three donor groups. (J) Young's modulus of neutrophils in three patients measured at two time
606 points: during COVID-19 and after recovery. Circle markers represent the median value, error bars
607 represent standard deviation. Statistical comparisons for (F-I) were done using Kruskal-Wallis test with
608 Dunn's posthoc test and for (J) using linear mixed model analysis, * $p < .05$, ** $p < .01$, *** $p < .001$.

609

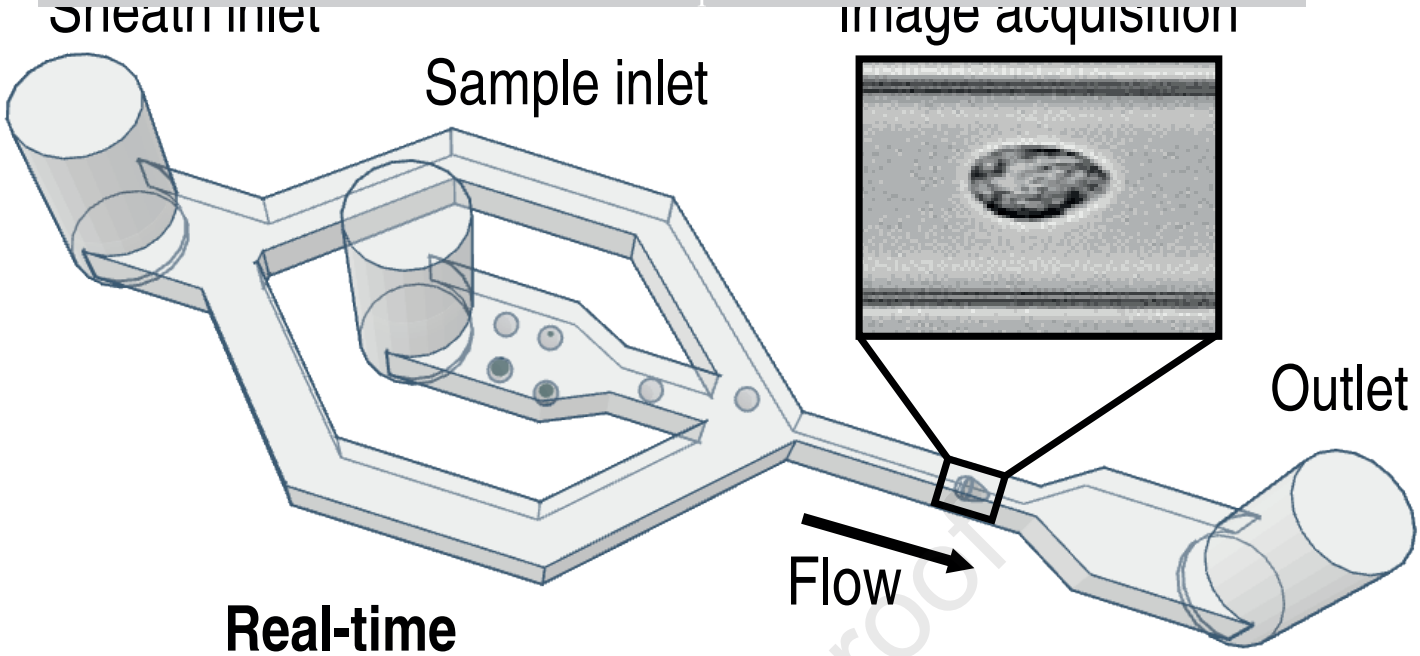


**Real-time deformability cytometry**

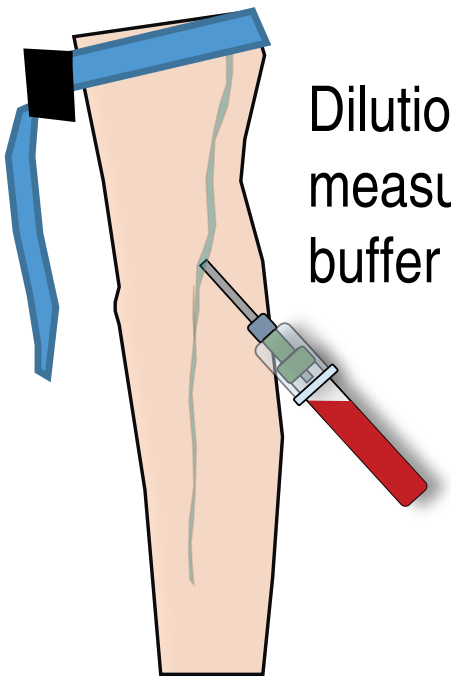

Dilution in measurement buffer 1:20

**Selection of cell population**

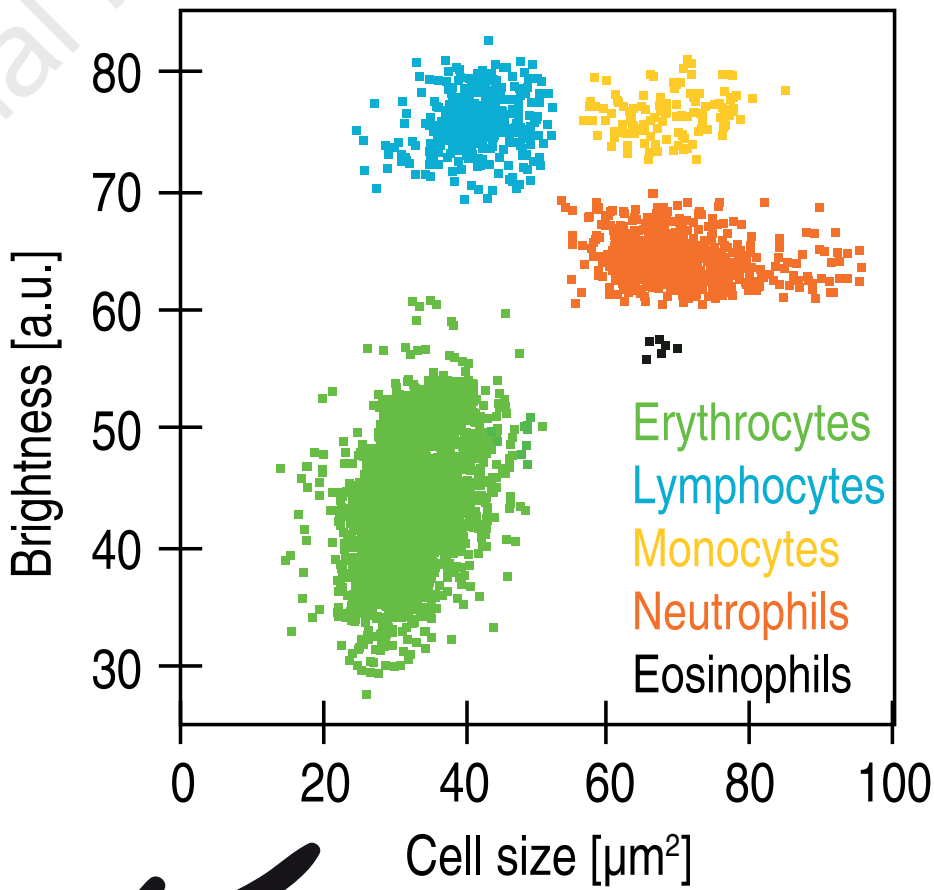


**Analysis of physical properties**

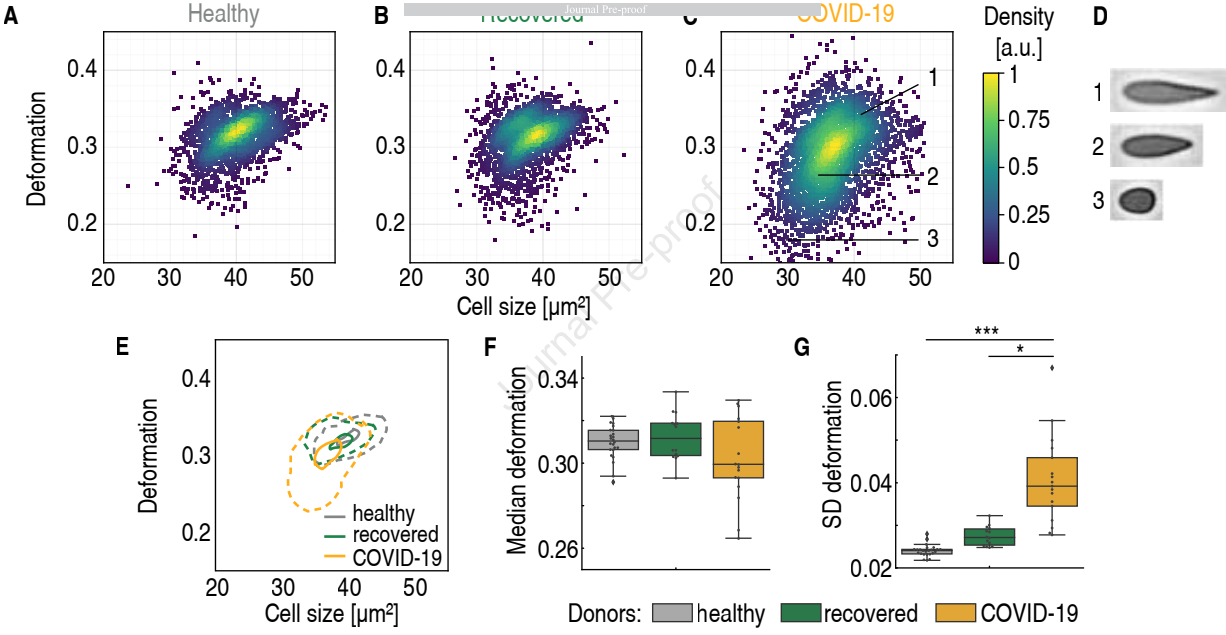
A
Healthy
B
Recovered
C
COVID-19
Density [a.u.]
1
0.75
0.5
0.25
0
D
Deformation
Cell size [μm²]
E
healthy
recovered
COVID-19
F
Median deformation
G
SD deformation
***
*
Donors: healthy recovered COVID-19

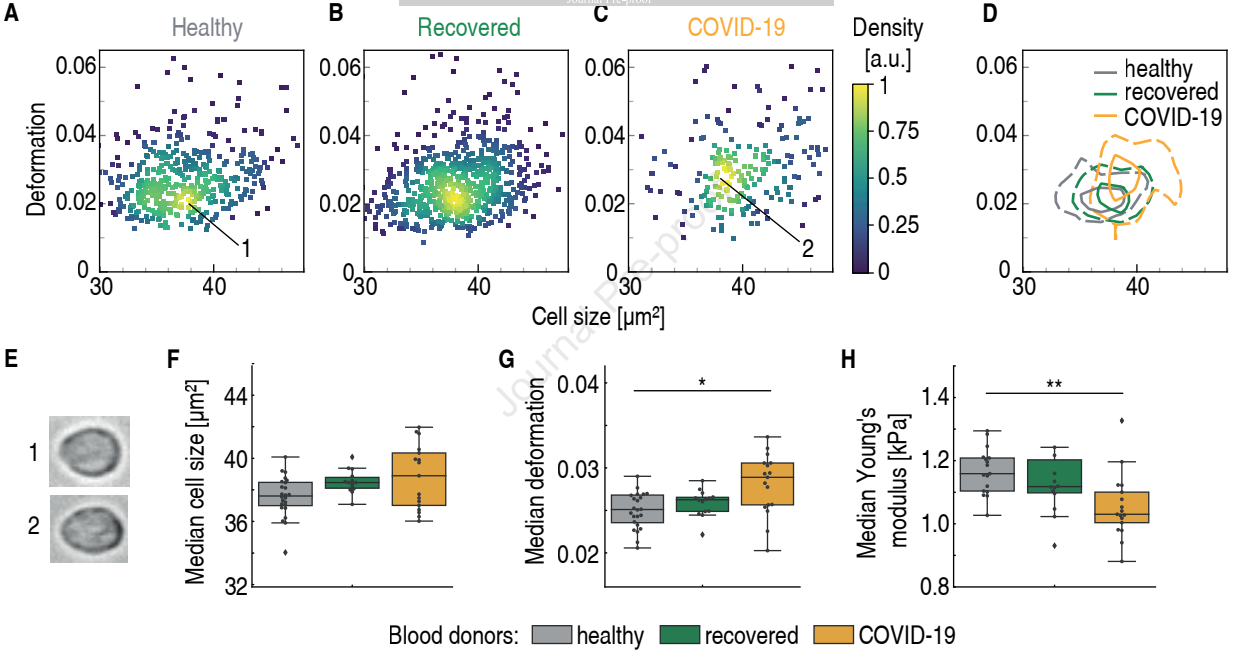

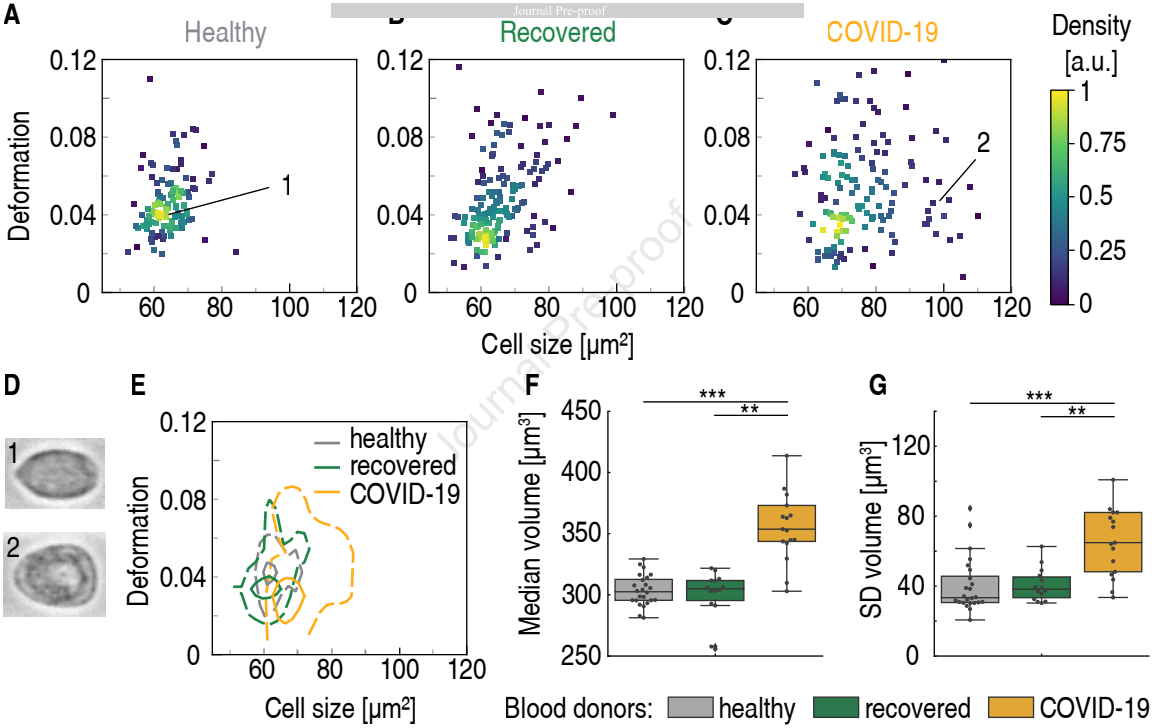

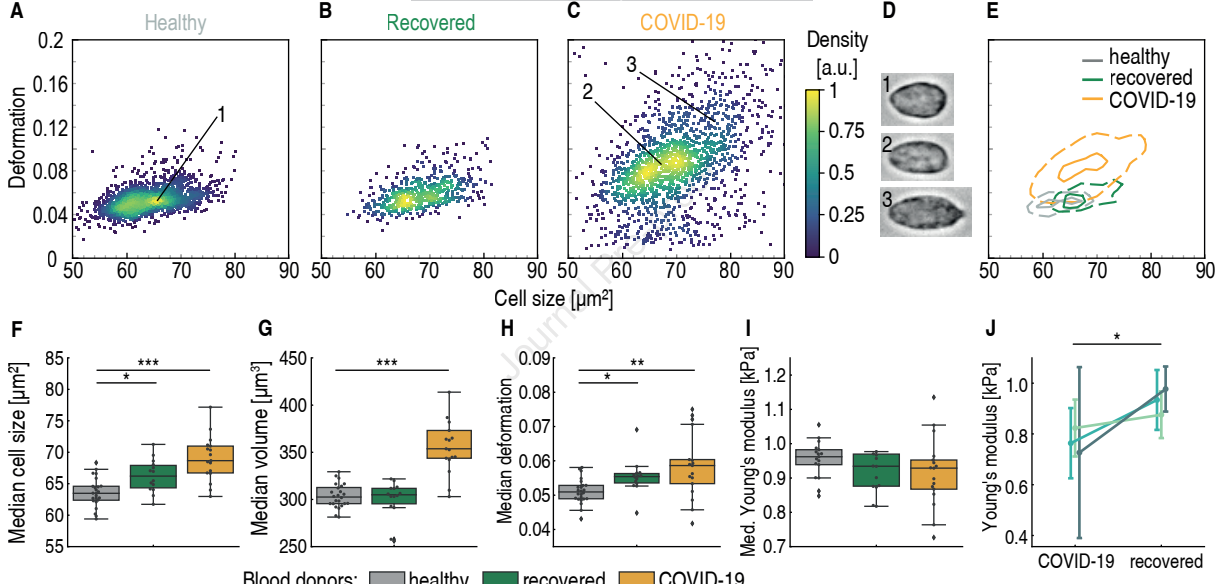

# Physical phenotype of blood cells is altered in COVID-19

**M Kubánková, B Hohberger, J Hoffmanns, J Fürst, M Herrmann, J Guck[#], M Kräter**

# corresponding author

1

## Supplementary Figures and Tables



**Supplementary table 1.** Patient characteristics, medical management and outcome of all donors included in this study.

| | All donors n=54 (100%) | | |
|---|---|---|---|
| | **Control n=24** | **Recovered n=14** | **COVID-19 n=17** |
| **Age (years): median (range)** | 62.5 ± 13.6 years (26-81) | 58.6 ± 12.4 (27-76) | 68·± 10.4 (41-87) |
| **Gender** | | | |
| male | 12 (50%) | 10 (71.4%) | 13 (76.5%) |
| female | 12 (50%) | 4 (18.6%) | 4 (23.5%) |
| **Primary virus identification (PCR airway)** | n.a. | 14 (100%) | 17 (100%) |
| **Complications and medical management** | | | |
| Oxygen supplementation | 0 | 0 | 17 (100%) |
| Mechanical ventilation | 0 | 0 | 13 (76.5%) |
| ECMO | 0 | 0 | 6 (35.3%) |
| Dialysis | 0 | 0 | 3 (17.6%) |
| Systemic Superinfection | 0 | 0 | 7 (41.1%) |
| Pulmonary embolism | 0 | 0 | 6 (35.3%) |
| **Drugs** | | | |
| Azithromycin | 0 | 0 | 3 (17.6%) |
| Hydroxychloroquine | 0 | 0 | 9 (52.9%) |
| Heparin prophylactic/therapeutic anticoagulation | 0 | 0 | 13 (76.5%) |
| **Outcome** | | | |
| Length of hospital stay (days) | 0 | 7 ± 2.4 (5-12) | 22.8 ± 14 (7-50) |
| Intensive care unit stay | 0 | 0 | 13 (76.5%) |
| Discharged | 0 | 14 (100%) | 9 (52.9%) |
| Further hospitalized | 0 | 0 | 0 |
| Death | 0 | 0 | 8 (47.1%) |

**Supplementary table 2.** Kruskal-Wallis *H*-statistics, *p*-values and effect sizes $\varepsilon^2$. The last three columns represent *p*-values from Dunn's posthoc tests conducted for the significant results of Kruskal-Wallis *H*-tests.

| A - healthy<br>B- recovered<br>C - COVID | *p* (Kruskal-Wallis) | *H* (Kruskal-Wallis) | $\varepsilon^2$ (Kruskal-Wallis) | *p* AC (Dunn's) | *p* AB (Dunn's) | *p* BC (Dunn's) |
|---|---|---|---|---|---|---|
| **Erythrocytes** | | | | | | |
| **Median area** | 0.1162 | 4.30 | 0.080 | 0.4896 | 0.1503 | 1.0000 |
| **SD area** | 0.0000 | 26.99 | 0.500 | 0.0000 | 0.2259 | 0.0112 |
| **Median volume** | 0.2532 | 2.75 | 0.051 | 1.0000 | 0.2938 | 1.0000 |
| **SD volume** | 0.0000 | 33.75 | 0.625 | 0.0000 | 0.9204 | 0.0002 |
| **Median deformation** | 0.2180 | 3.05 | 0.056 | 0.4480 | 1.0000 | 0.3380 |
| **SD deformation** | 0.0000 | 42.30 | 0.783 | 0.0000 | 0.0024 | 0.0340 |
| **% of ery with def < 0.28** | 0.0000 | 25.83 | 0.478 | 0.0000 | 1.0000 | 0.0016 |
| **Neutrophils** | | | | | | |
| **Median area** | 0.0000 | 22.95 | 0.425 | 0.0000 | 0.2704 | 0.0260 |
| **SD area** | 0.0001 | 18.86 | 0.349 | 0.0023 | 0.0001 | 0.6791 |
| **Median volume** | 0.0000 | 23.53 | 0.436 | 0.0000 | 0.1319 | 0.0517 |
| **SD volume** | 0.0001 | 19.78 | 0.366 | 0.0005 | 0.0002 | 1.0000 |
| **Median deformation** | 0.0013 | 13.31 | 0.246 | 0.0021 | 1.0000 | 0.0319 |
| **SD deformation** | 0.0059 | 10.28 | 0.190 | 0.0041 | 0.3772 | 0.5059 |
| **Median Young's modulus** | 0.1698 | 3.55 | 0.066 | 0.1827 | 1.0000 | 0.8807 |
| **Lymphocytes** | | | | | | |
| **Median area** | 0.0499 | 6.00 | 0.111 | 0.1667 | 1.0000 | 0.0939 |
| **SD area** | 0.0000 | 30.78 | 0.570 | 0.2270 | 0.0010 | 0.0000 |
| **Median volume** | 0.0814 | 5.02 | 0.093 | 0.3403 | 1.0000 | 0.1134 |
| **SD volume** | 0.0000 | 28.36 | 0.525 | 0.7403 | 0.0003 | 0.0000 |
| **Median deformation** | 0.0132 | 8.66 | 0.160 | 0.0107 | 0.1945 | 1.0000 |
| **SD deformation** | 0.0000 | 35.61 | 0.659 | 0.0043 | 0.0218 | 0.0000 |
| **Median Young's modulus** | 0.0029 | 11.68 | 0.216 | 0.0029 | 0.0542 | 1.0000 |
| **Monocytes** | | | | | | |
| **Median area** | 0.0000 | 30.64 | 0.567 | 0.0000 | 0.0001 | 1.0000 |
| **SD area** | 0.0011 | 13.65 | 0.253 | 0.0007 | 0.0892 | 0.7682 |
| **Median volume** | 0.0000 | 27.71 | 0.513 | 0.0000 | 0.0001 | 1.0000 |
| **SD volume** | 0.0001 | 18.48 | 0.342 | 0.0001 | 0.0075 | 1.0000 |
| **Median deformation** | 0.7918 | 0.47 | 0.009 | 1.0000 | 1.0000 | 1.0000 |
| **SD deformation** | 0.4949 | 1.41 | 0.026 | 0.7256 | 1.0000 | 1.0000 |
| **Median Young's modulus** | 0.7763 | 0.51 | 0.009 | 1.0000 | 1.0000 | 1.0000 |
| **Eosinophils** | | | | | | |
| **Median area** | 0.1289 | 4.10 | 0.076 | 0.6099 | 0.1547 | 1.0000 |
| **SD area** | 0.0126 | 8.7600 | 0.162 | 0.1245 | 0.0168 | 1.0000 |
| **Median volume** | 0.2532 | 2.75 | 0.051 | 1.0000 | 0.2938 | 1.0000 |
| **SD volume** | 0.0000 | 33.75 | 0.625 | 0.0000 | 0.9204 | 0.0002 |
| **Median deformation** | 0.4143 | 1.76 | 0.033 | 1.0000 | 0.9095 | 0.5981 |
| **SD deformation** | 0.5965 | 1.03 | 0.019 | 1.0000 | 1.0000 | 0.9290 |
| **Median Young's modulus** | 0.9592 | 0.08 | 0.002 | 1.0000 | 1.0000 | 1.0000 |
| **% of WBC** | | | | | | |
| **% neutrophils** | 0.0105 | 9.10 | 0.169 | 0.0499 | 1.0000 | 0.0174 |
| **% lymphocytes** | 0.0007 | 14.63 | 0.271 | 0.0006 | 0.2426 | 0.0328 |
| **% monocytes** | 0.0151 | 8.38 | 0.155 | 0.0244 | 1.0000 | 0.0644 |
| **% eosinophils** | 0.0010 | 13.73 | 0.254 | 0.1576 | 0.0007 | 0.1970 |
| **NLR** | 0.0022 | 12.22 | 0.226 | 0.0031 | 0.7018 | 0.0252 |

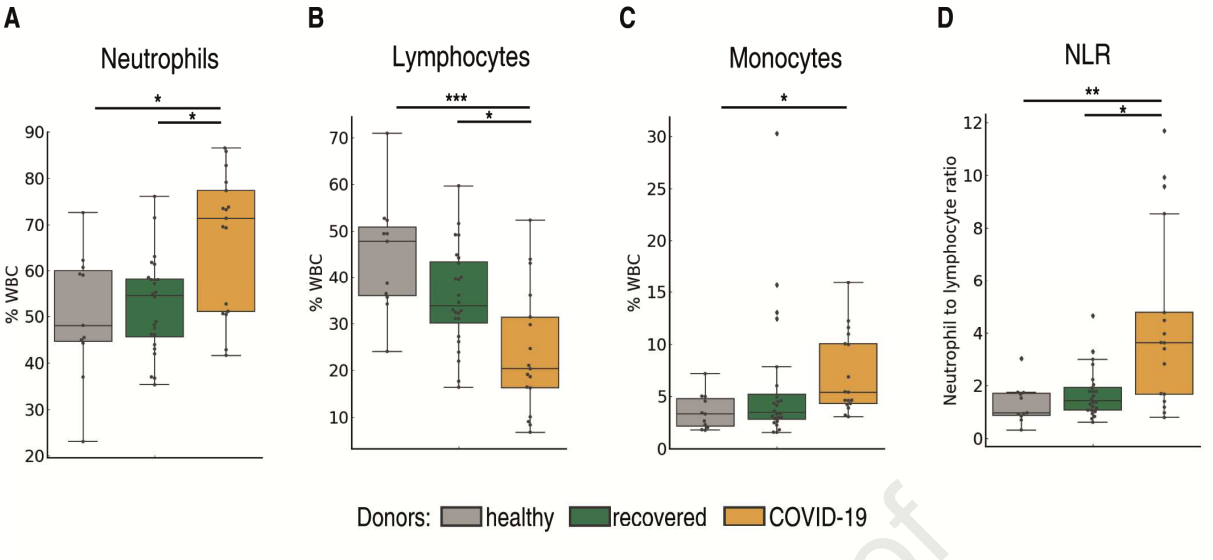


**Supplementary figure 1. Proportions of white blood cells calculated from real-time deformability cytometry (RT-DC) data.** The percentage of A) neutrophils, B) lymphocytes and C) monocytes in the total white blood cell count; a comparison of the control blood donor cohort (grey), recovered patients (green) and hospitalized COVID-19 patients (yellow). D) The neutrophil to lymphocyte ratio is significantly higher in hospitalized patients compared to the recovered and healthy donor cohorts, * $p < .05$, ** $p < .01$, *** $p < .001$.

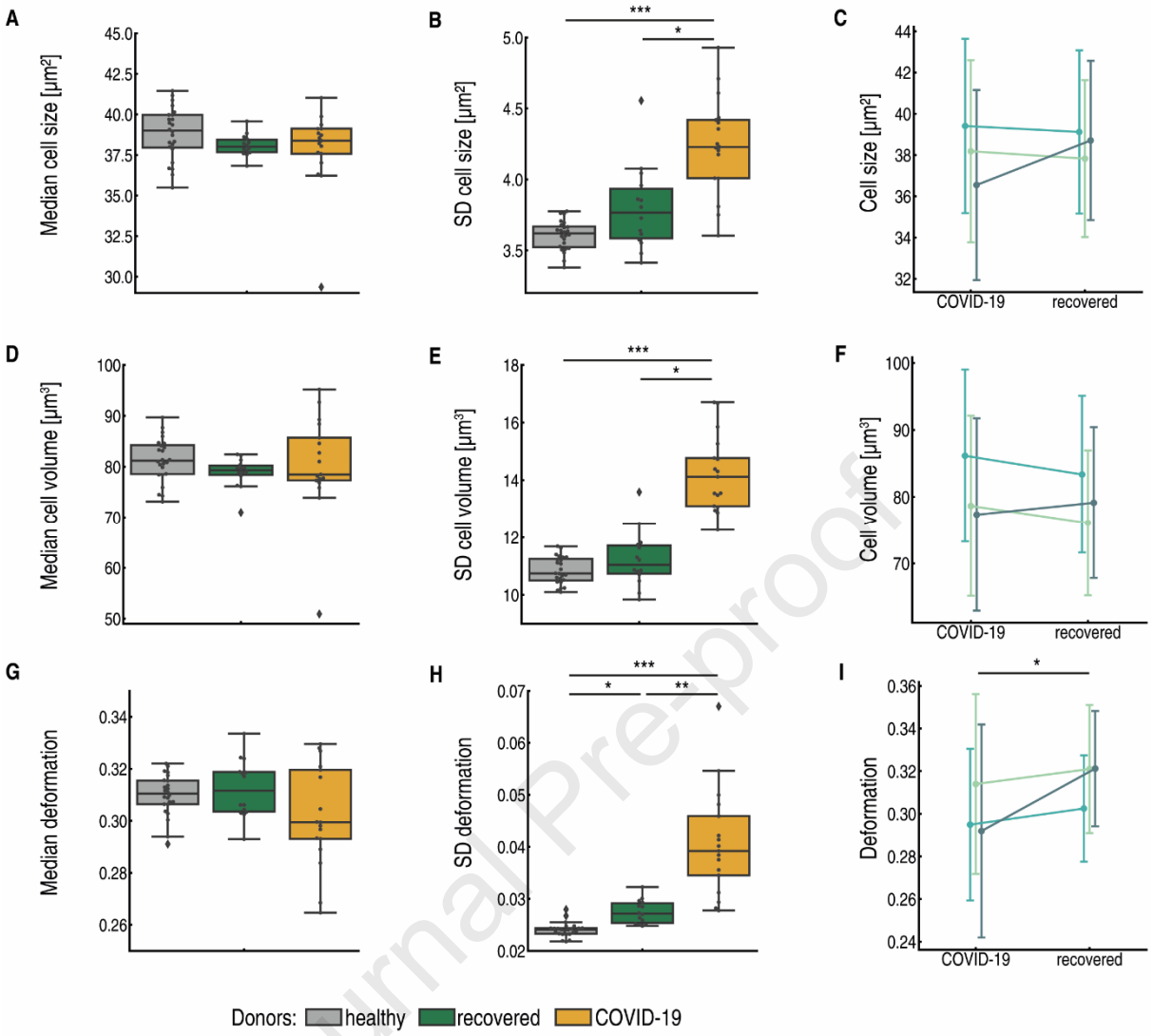


**Supplementary figure 2. Physical properties of erythrocytes of COVID-19 patients compared to controls.** Quantification of A-C) cross-sectional cell area, D-F) cell volume, G-I) cell deformation; in these graphs COVID-19 patients (yellow, n = 17) are compared to recovered donors (green, n = 14) and healthy donors (grey, n = 24). Panels C), F), I) show three patients measured at two time points, during COVID-19 and after recovery; circle markers represent the median value and error bars represent the standard deviation for each patient. Statistical comparisons in C), F), I) were performed using linear mixed model analysis. All other statistical comparisons were done using Kruskal-Wallis test with Dunn's posthoc test. * $p < .05$, ** $p < .01$, *** $p < .001$.

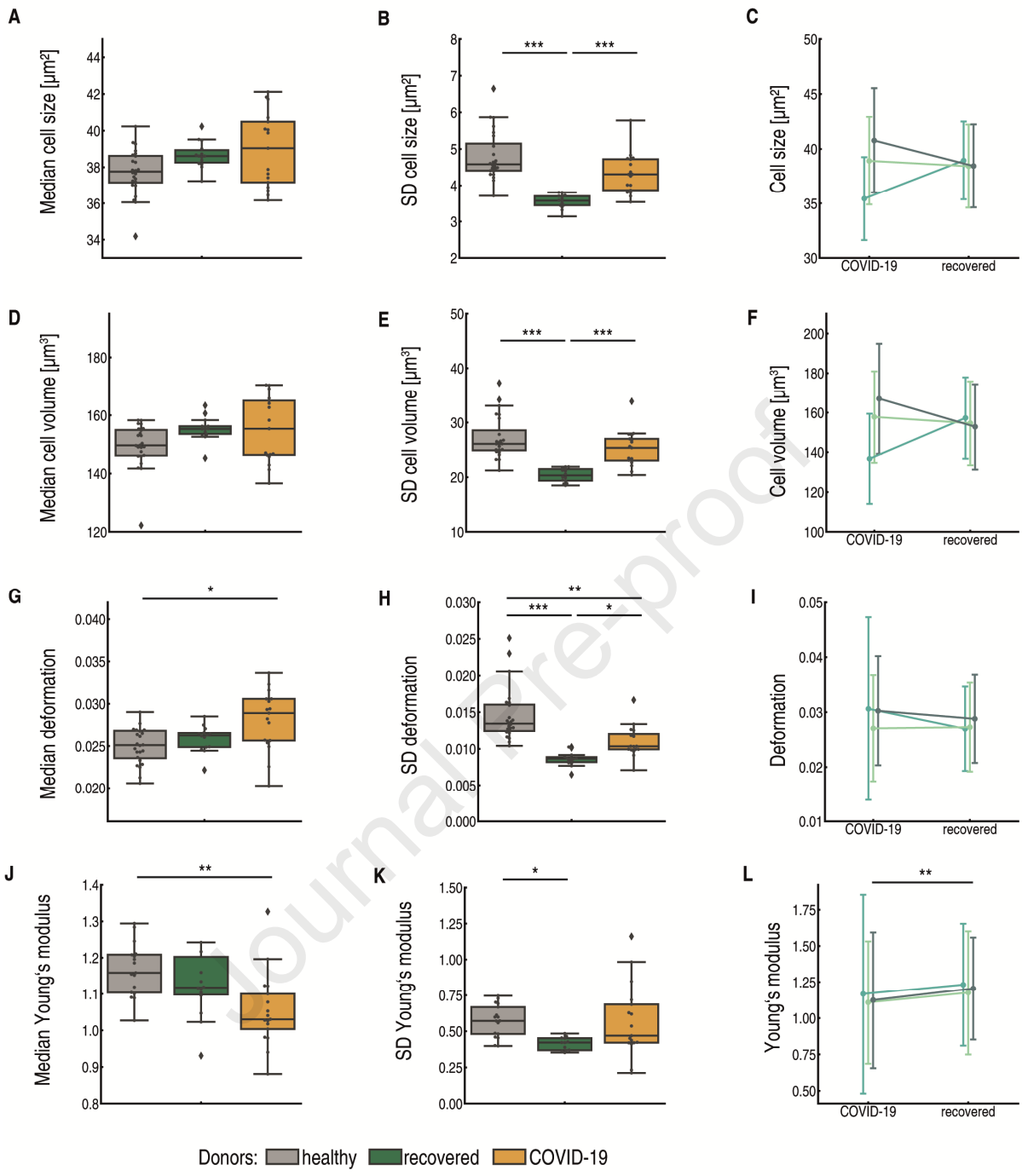


**Supplementary figure 3. Physical properties of lymphocytes of COVID-19 patients compared to controls.** Quantification of A-C) cross-sectional cell area, D-F) cell volume, G-I) cell deformation, J-L) Young's modulus; in these graphs COVID-19 patients (yellow, n = 17) are compared to recovered donors (green, n = 14) and healthy donors (grey, n = 24). Panels C), F), I) and L) show three patients measured at two time points, during COVID-19 and after recovery; circle markers represent the median value and error bars represent the standard deviation for each patient. Statistical comparisons in C), F), I), L) were performed using linear mixed model analysis. All other statistical comparisons were done using Kruskal-Wallis test with Dunn's posthoc test. * $p < .05$, ** $p < .01$, *** $p < .001$.

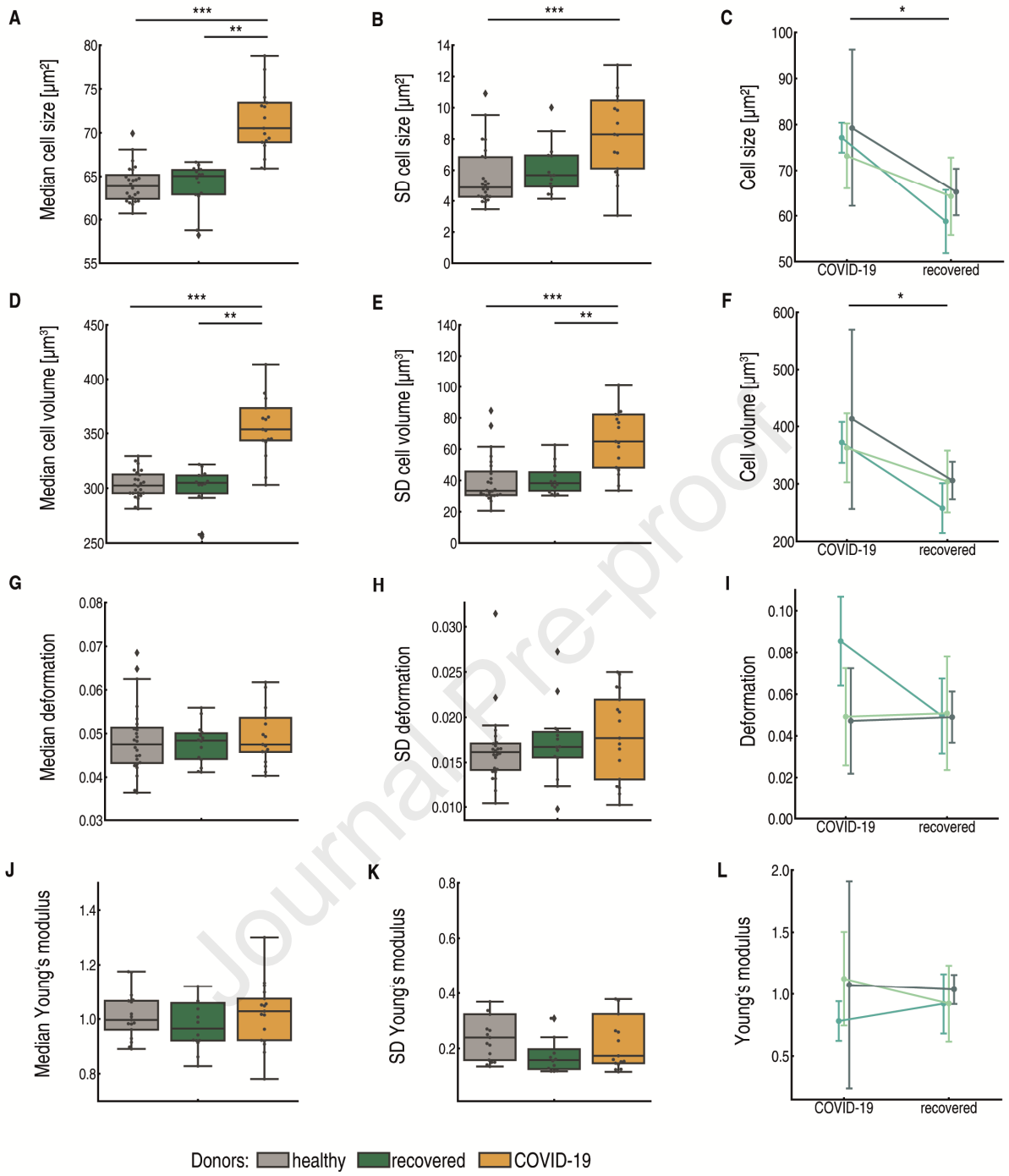




**Supplementary figure 4. Physical properties of monocytes of COVID-19 patients compared to controls.** Quantification of A-C) cross-sectional cell area, D-F) cell volume, G-I) cell deformation, J-L) Young's modulus; in these graphs COVID-19 patients (yellow, n = 17) are compared to recovered donors (green, n = 14) and healthy donors (grey, n = 24). Panels C), F), I) and L) show three patients measured at two time points, during COVID-19 and after recovery; circle markers represent the median value and error bars represent the standard deviation for each patient. Statistical comparisons in C), F), I), L) were performed using linear mixed model analysis. All other statistical comparisons were done using Kruskal-Wallis test with Dunn's posthoc test. * $p < .05$, ** $p < .01$, *** $p < .001$.

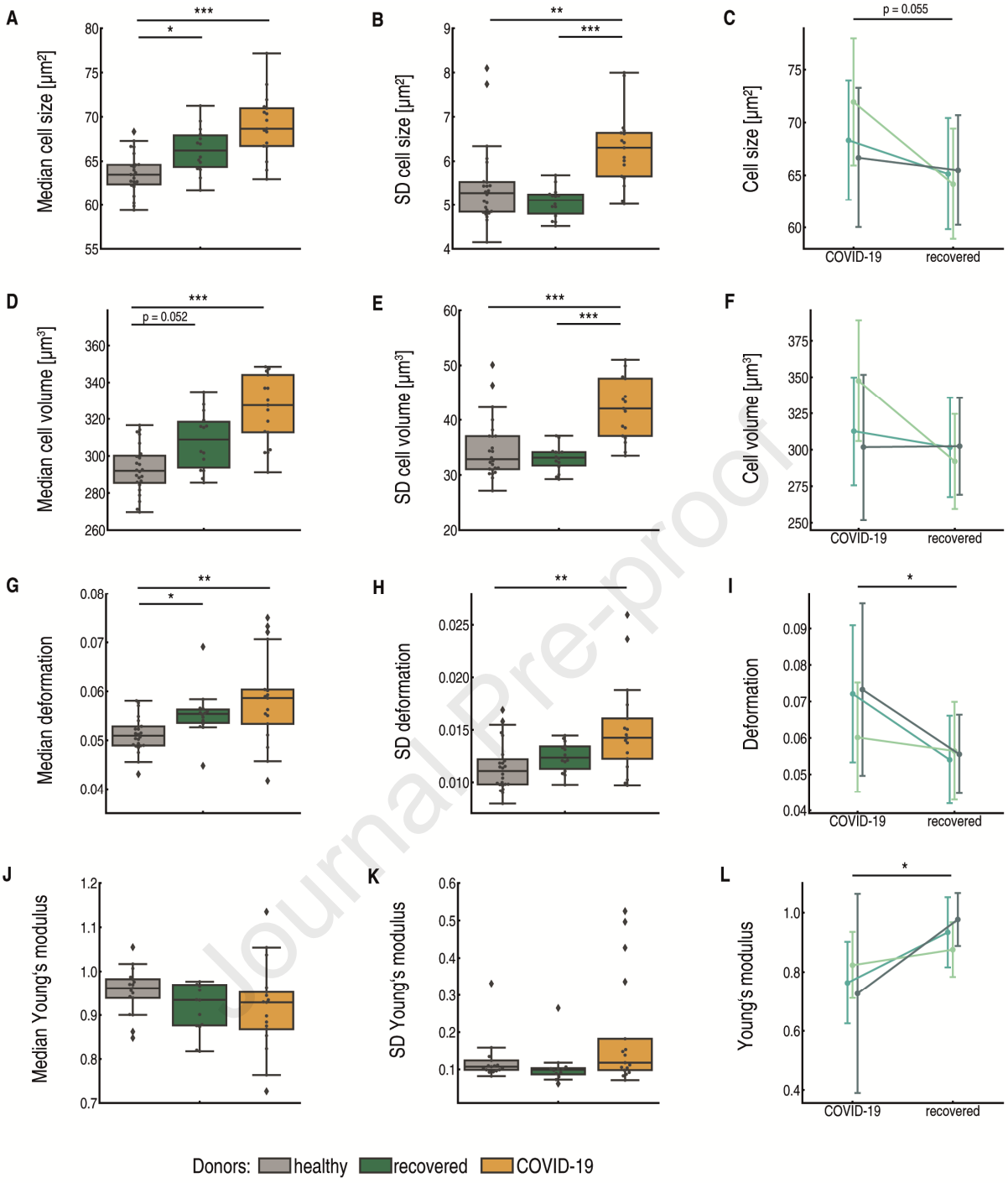


**Supplementary figure 5. Physical properties of neutrophils of COVID-19 patients compared to controls.** Quantification of A-C) cross-sectional cell area, D-F) cell volume, G-I) cell deformation, J-L) Young's modulus; in these graphs COVID-19 patients (yellow, n = 17) are compared to recovered donors (green, n = 14) and healthy donors (grey, n = 24). Panels C), F), I) and L) show three patients measured at two time points, during COVID-19 and after recovery; circle markers represent the median value and error bars represent the standard deviation for each patient. Statistical comparisons in C), F), I), L) were performed using linear mixed model analysis. All other statistical comparisons were done using Kruskal-Wallis test with Dunn's posthoc test. * $p < .05$, ** $p < .01$, *** $p < .001$.

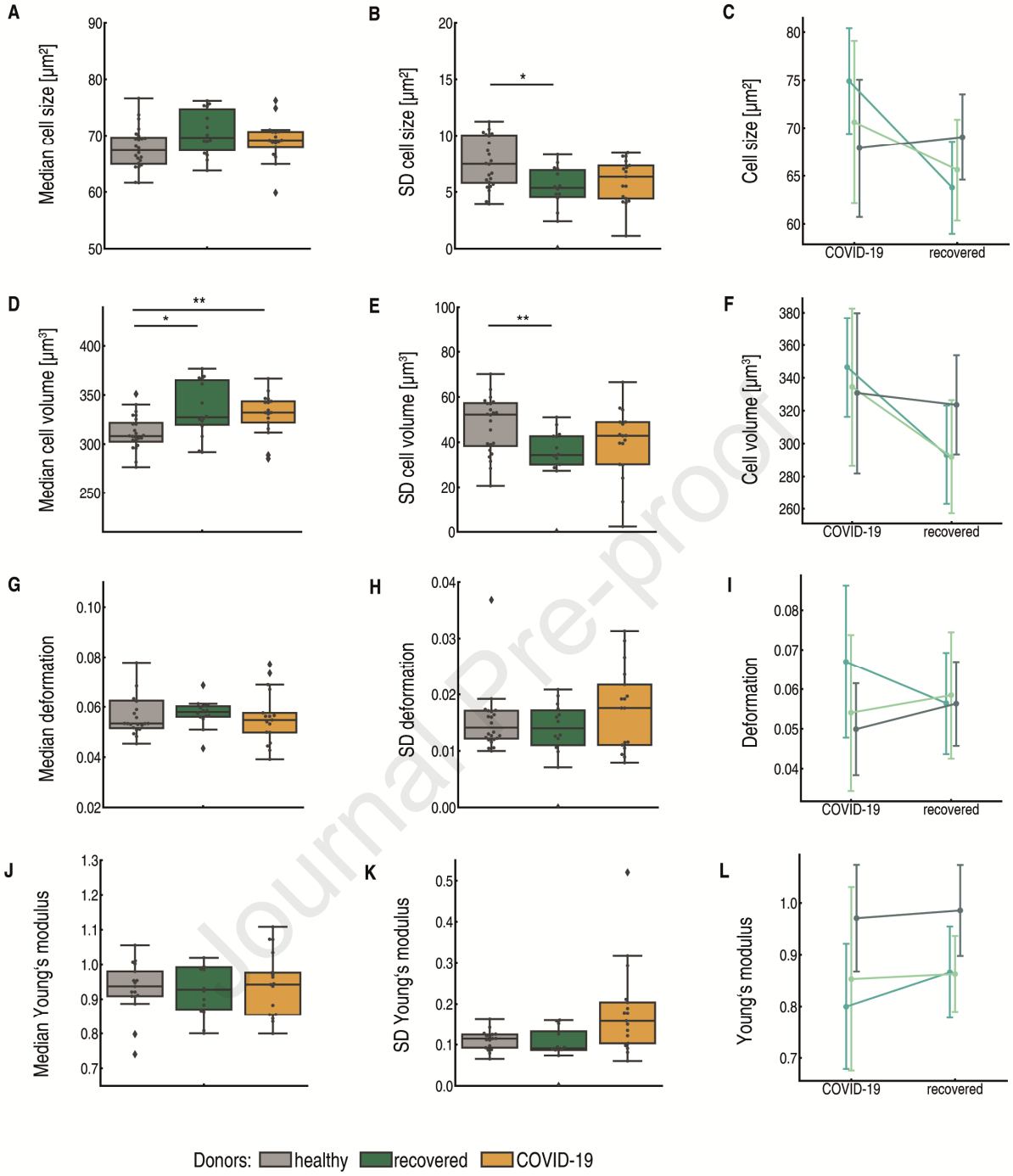


**Supplementary figure 6. Physical properties of eosinophils of COVID-19 patients compared to controls.** Quantification of A-C) cross-sectional cell area, D-F) cell volume, G-I) cell deformation, J-L) Young's modulus; in these graphs COVID-19 patients (yellow, n = 17) are compared to recovered donors (green, n = 14) and healthy donors (grey, n = 24). Panels C), F), I) and L) show three patients measured at two time points, during COVID-19 and after recovery; circle markers represent the median value and error bars represent the standard deviation for each patient. Statistical comparisons in C), F), I), L) were performed using linear mixed model analysis. All other statistical comparisons were done using Kruskal-Wallis test with Dunn's posthoc test. * $p < .05$, ** $p < .01$, *** $p < .001$.

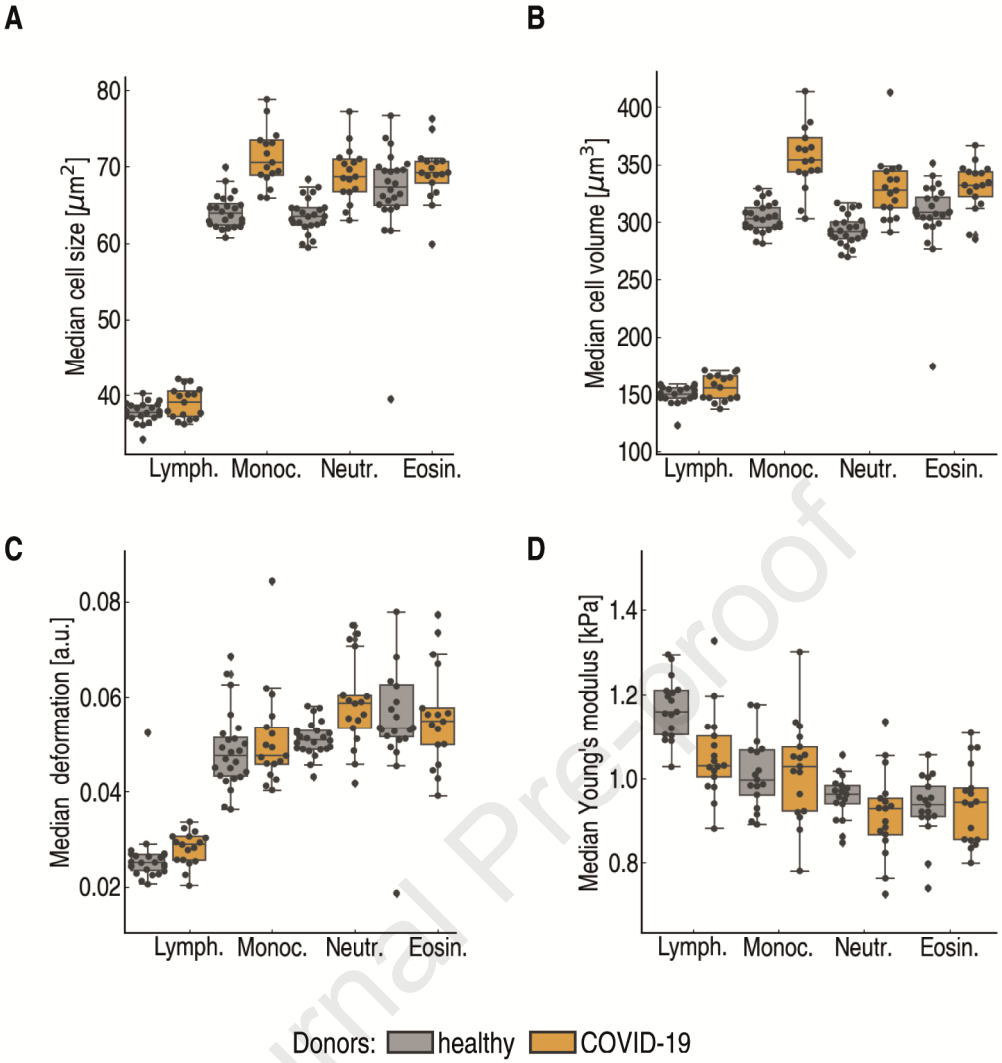


63

64 **Supplementary figure 7. A comparison of the physical properties of the four examined white blood**
65 **cell types in COVID-19 patients (yellow) compared to the control group (grey).** A) Median cell size,
66 B) median cell volume, C) median deformation, D) median Young's modulus.